Dose Rate Effects in Fluorescence Chemical Dosimeters Exposed to Picosecond Electron Pulses: An Accurate Measurement of Low Doses at High Dose Rates

Authors: Precek, Martin, Kubelik, Petr, Vysin, Ludek, Schmidhammer, Uli, Larbre, Jean-Philippe, et al.

Source: Radiation Research, 197(2) : 131-148

Published By: Radiation Research Society

URL: https://doi.org/10.1667/RADE-20-00292.1

RADIATION RESEARCH **197**, 131–148 (2022)
0033-7587/22 $15.00

DOI: 10.1667/RADE-20-00292.1

Dose Rate Effects in Fluorescence Chemical Dosimeters Exposed to Picosecond Electron Pulses: An Accurate Measurement of Low Doses at High Dose Rates

Martin Precek,[a,b,1] Petr Kubelik,[b,c] Ludek Vysin,[b] Uli Schmidhammer,[d] Jean-Philippe Larbre,[d] Alexandre Demarque,[d] Pierre Jeunesse,[d] Mehran Mostafavi[d] and Libor Juha[b,e]

[a] *ELI Beamlines, Institute of Physics, Czech Academy of Sciences, Za Radnicí 835, 252 41 Dolní Břežany, Czech Republic;* [b] *Department of Radiation and Chemical Physics, Institute of Physics, Czech Academy of Sciences, Na Slovance 1999/2, 18221 Prague, Czech Republic;* [c] *Department of Spectroscopy, J. Heyrovsky Institute of Physical Chemistry, Czech Academy of Sciences, Dolejškova 2155/3, 182 23 Prague 8, Czech Republic;* [d] *Institut de Chimie Physique/ELYSE, CNRS UMR 8000, Université Paris-Saclay, 91400 Orsay, France; and* [e] *Laser Plasma Department, Institute of Plasma Physics, Czech Academy of Sciences, Za Slovankou 1782/3, 18200 Prague, Czech Republic*

Precek M., Kubelik P., Vysin L., Schmidhammer U., Larbre J-P., Demarque A., Jeunesse P., Mostafavi M. and Juha L. Dose Rate Effects in Fluorescence Chemical Dosimeters Exposed to Picosecond Electron Pulses: An Accurate Measurement of Low Doses at High Dose Rates. *Radiat. Res*. 197, 131–148 (2022).

The development of ultra-intense electron pulse for applications needs to be accompanied by the implementation of a practical dosimetry system. In this study four different systems were investigated as dosimeters for low doses with a very high-dose-rate source. First, the effects of ultra-short pulses were investigated for the yields of the Fricke dosimeter based on acidic solutions of ferrous sulfate; it was established that the yields were not significantly affected by the high dose rates, so the Fricke dosimeter system was used as a reference. Then, aqueous solutions of three compounds as fluorescence chemical dosimeters were utilized, each operated at a different solution pH: terephthalic acid - basic, trimesic acid - acidic, and coumarin-3-carboxylic acid (C3CA) - neutral. Fluorescence chemical dosimeters offer an attractive alternative to chemical dosimeters based on optical absorption for measuring biologically relevant low doses because of their higher sensitivity. The effects of very intense dose rate (TGy/s) from pulses of fast electrons generated by a picosecond linear accelerator on the chemical yields of fluorescence chemical dosimeters were investigated at low peak doses (<20 Gy) and compared with yields determined under low-dose-rate irradiation from a 60 Co gamma-ray source (mGy/s). For the terephthalate and the trimesic acid dosimeters changes in the yields were not detected within the estimated (~10%) precision of the experiments, but, due to the complexity of the mechanism of the hydroxyl radical initiated reactions in solutions of the relevant aromatic compounds, significant reductions of the chemical yield (–60%) were observed when the C3CA dosimeter was irradiated with the ultra-short pulses. © 2022 by Radiation Research Society

INTRODUCTION

Dose Rate Effects in Liquid Chemical Dosimeters

In the past 2–3 decades, implementation of new ultrashort pulsed sources of radiation, X-ray free electron lasers (1, 2), plasma X-ray sources (3) and accelerated charged particles (4–6) was made possible thanks to the widespread availability of ultra-fast laser beam technology. These new sources are capable of producing pulses of ionizing radiation as short as few femtoseconds and, in the case of X-rays, even shorter (7, 8). Efforts are under way to apply these new sources of radiation in radiobiological studies and, eventually, in radiotherapy applications (9, 10). Although the desirable doses for these applications are relatively low ($<10^2$ Gy) the ultrashort character of the pulses results in extremely high dose rates ($>10^{12}$ Gy/s). This poses a challenge to established dosimetric systems in that they will need to be investigated and adjusted for the ultrashort character of the administered pulses that are many orders of magnitude shorter compared to classical irradiation sources.

It is widely acknowledged that chemical dosimeter systems experience significant changes of their chemical radiolytic yield when the type of ionizing radiation is changed (e.g., between fast electrons and soft X-ray photons), primarily as a result of different linear energy transfer (LET) (11, 12). However, what is substantially less established is the range of dose rates where the radiolytic yields of the chemical species important for the working of the dosimeter can be assumed to be independent. If the

Editor's note. The online version of this article (DOI: https://doi.org/10.1667/RADE-20-00292.1) contains supplementary information that is available to all authorized users.

[1] Address for correspondence: ELI Beamlines, Institute of Physics, Czech Academy of Sciences, Za Radnicí 835, 252 41 Dolní Břežany Czech Republic; email: martin.precek@gmail.com.

already developed chemical dosimeter systems need to be utilized with picosecond and sub-picosecond sources, then the independence from changes of dose rate must be verified.

Fricke Dosimeter

The Fricke dosimeter, based on aqueous solutions of $\sim 10^{-3}$ M Fe^{2+} in sulfuric acid is one of a few systems that were systematically investigated for the effect of very high dose rates from pulsed sources (13–19). These investigations were performed using pulses of fast electrons from linear accelerators, where the length of the pulses was on the order of 10^{-6} s and the pulse was capable of delivering a dose on the order of 10^2–10^3 Gy to the liquid samples – this way the achievable dose rates were multiple orders of magnitudes higher than from the best available radionuclide sources. Up to the dose rate of approximately 10^5–10^6 Gy/s ($0.62 \times [10^{24}$–$10^{25}]$ $eV.L^{-1}.s^{-1}$, as recalculated to units utilized in the older studies), the chemical yields were found to be independent of dose rate, close to the value of 1.62 μmol/J (=15.6 ions/100 eV). At higher dose rates, the Fricke dosimeter started to reveal decreasing chemical yields, dropping by about 40% at dose rates around 10^9 Gy/s ($\approx 10^{28}$ $eV.L^{-1}.s^{-1}$). Attempts were made to alleviate this effect by modifying the dosimeter, by increasing the oxygenation of the solutions, or by increasing the total ferrous iron concentration, but were ultimately only marginally successful (18). However, as has been reasoned by Rotblat and Sutton (15), the main reason for such a large drop in the yield of the Fricke dosimeter in these studies was likely from the total value of the dose per pulse rather than simply the dose rate. For the $\sim 10^{-6}$ s linac pulses, Rotblat and Sutton ascribe more significance to expression of dose rate as ''dose per pulse'' rather than ''dose per unit of time''; they also noted that it was essential to avoid peak dose in excess of 400 Gy to avoid oxygen depletion, which manifested by a sharp drop of chemical yield at approximately 600–800 Gy. Experiments with progression of cumulative doses up to 2,000 Gy delivered by 80–200 Gy pulses have reproduced this effect regardless of the spacing between the pulses in the range 0.0025 to 1 s. With pulses >1 μs long, it is clear that in the studies where dose rates of the order of 10^9 Gy/s were achieved (18), doses of the order of 1,000 Gy/pulse had to be utilized, which caused oxygen depletion (in solutions equilibrated with air) and – consequently – to the reported substantial drop in dosimeter yield.

A less prominent effect, yet measurable, reduction of Fe^{3+} yields was observed already for smaller peak doses with $G(Fe^{3+})$. The yield dropped by approximately 5% at a ''dose rate'' of already 10 Gy/pulse ($\sim 10^7$ Gy/s), the change becoming less significant when initial concentrations of dissolved oxygen and of ferrous sulphate were increased (15). These investigations have, hence, revealed the limits of practical usage of the dosimeter for highly intense pulses of ionizing radiation.

The topic has not been researched exhaustively, recent investigations of O'Leary et al. (20) with approximately tenfold higher LET radiation in the form of monochromatic 20 keV synchrotron X rays indicate that a slight decrease in the yields of the Fricke dosimeter can manifest already when the dose rate is increased in the range from 10^2–10^3 Gy/s (a drop of 10% was detected when average doses below 500 Gy were administered; for doses above 500 Gy, the effect of oxygen depletion - a fast drop of the yield - was observed as well). In addition, a recent investigation using ultra-soft X rays in the energy range of the so-called water window (284–543 eV) generated by laser driven plasma, where the dose rate in the pulsed regime reached an order of 10^6 Gy/s, has reported a substantial decrease in the yield of ferric ions (21). Nonetheless, since water-window X rays have a very high LET, it is less straightforward to compare these results with the low-LET systems mentioned above and utilized in this study.

The standard Fricke dosimeter system relies on measuring the change of transmittance of the liquid solution at a wavelength of 304 nm caused by the radiolytic oxidation of Fe^{2+} to Fe^{3+}. At this wavelength, a dose of 1 Gy of low-LET radiation (primarily high energy electrons and photons) causes an increase in absorbance of solution measured in a standard 1-cm pathlength cuvette by 0.0036 (at 25°C) (22). Such a small increase in absorbance translates to a 0.83% decrease in transmittance, which is too little to perform reliable quantitation in most circumstances. For this reason, the recommended range for measuring doses is between 20–400 Gy; however, with some modifications of the nominally 1 mM Fe^{2+} solution can allow its deployment for higher doses (up to 2,000 Gy) (23, 24). Some modifications to the Fricke dosimeter, e.g., the addition of a significant concentration of cupric ions (up to 10^{-1} M Cu^{2+}) that significantly depress the chemical yield of Fe^{3+} after irradiation, could potentially extend the practical working range even further; however, the dose rate sensitivity has not been established.

Modifications of the Fricke dosimeter towards the opposite range of doses, e.g., for measuring small doses, exist as well. These mostly involve the use of metal ion indicator compounds that – when combined with Fe^{3+} ions – develop very deep absorption bands. The best established system is the FBX dosimeter (25), based on additions of xylenol orange as indicator and benzoic acid as radical yield amplifier to the ferrous sulfate – sulfuric acid system. The advantage of the system is an approximately 30× higher sensitivity to radiation dose. Disadvantages are that the response is non-linear with dose and fairly strict control on the time of measurement after irradiation is required for best accuracy (26), also the effects for high dose rates above 10 Gy/s have not yet been established (27, 28), while at very low dose rates (<0.01 Gy/h) the dosimeter has significant changes in chemical yields (29).

Fluorescence Dosimeters

Chemical dosimetry based on radiation-induced fluorescence in liquid samples has been recently attracting the interest of the radiation research community (30–33). It presents an alternative to absorption based liquid chemical dosimeters because it allows us to reliably extend liquid chemical dosimetry to the area of low doses, below 10^{-1} Gy, while also widening the range of accurately measurable doses.

Compared to well-founded chemical dosimetry based on optical absorption [e.g., the ferrous sulphate Fricke or the ceric-cerous sulfate dosimeters (26)], fluorescence dosimetry has the advantage of offering higher sensitivity to lower dose, because the detection of the fluorescence emission signal can be in favorable conditions performed as free of background baseline signal and therefore, amplified by either increasing the power of the excitation light or by integration of a very weak signal, which is a method that does not help in absorption spectrophotometry (34), where baseline reproducibility, flatness and stability complicates the measurement of small absorbance signals (35). Another advantage is that fluorescence detection, as well as other emission based methods, can be performed in an off-axis geometry (usually in a 90° angle to the excitation light) (35), which makes it possible to be combined with other inspection methods simultaneously. In addition, the required combination of both excitation and emission wavelengths offers somewhat enhanced detection specificity. These benefits are of course countered by several disadvantages – the primary being the need to perform proper calibration of the emission detection system using reference standards; secondarily, one has to cope with the inner filter effect in excitation, secondary absorption of the emission, photobleaching and Raman scattering of the solvent (36).

Research into fluorescence chemical dosimeters started at the end of the 1950s, initially with the approach of radiolytic destruction of fluorescent quinine (37), observed as an exponential decrease. Although this method side-steps the need for a reference fluorescent compound during analysis, the concentrations of the fluorescent molecules are relatively small (10^{-8} to 10^{-5} mol/L), so the presence of impurities can interfere with dosimetry due to parasitic scavenging of the radicals that cause the destruction of the fluorescent compound. Hence, methods that continued in their development were based on more concentrated solutions ($>10^{-5}$ mol/L) of (usually) non-fluorescent compounds that upon irradiation produced a fluorescent product (26). The best studied systems of fluorescence chemical dosimeters are aqueous solutions of aromatic compounds, e.g., benzoic acid (38, 39), that upon irradiation create species with fluorescent activity by reacting with $^{\bullet}OH$ generated by water radiolysis. These systems are also used as probes for hydroxyl radicals in applications outside of radiation dosimetry, e.g. study of cellular metabolism (40) and ultrasound dosimetry (41–44).

A much less investigated group of compounds for liquid fluorescence chemical dosimetry is based on interaction with the reducing radiolytic species, primarily the solvated electron. So far, only compounds of resazurin have been investigated with this intention (45, 46).

For the present study, three dosimeter systems were chosen – aqueous solutions of terephthalic acid, trimesic acid and coumarin-3-carboxylic acid. The advantage of these systems is that they were all relatively well studied in the past. The main distinction between them is that their recommended compositions cover three different areas of solution pH (respectively, basic, acidic, and neutral).

Terephthalate Dosimeter

Alkalic solution of terephthalic acid (benzene-1, 4-dicarboxylic acid) is one of the first systems which has been studied with the intention of use for fluorescence dosimetry applications (47). A number of studies have been carried out to determine its performance as dosimeter for ionizing radiation (48–50). The best studied composition of the terephthalate (TA) dosimeter is usually prepared as an aerated aqueous solution of 1×10^{-4} M terephthalic acid in 4×10^{-4} M NaOH (48). The sensitive molecule is present in the form of the terephthalate anion, since in the basic solutions the terephthalic acid molecule is completely deprotonated ($pKa_1 = 3.54$, $pKa_2 = 4.34$) (51). Lowering the pH is not advisable, because the limit of solubility of the protonated terephthalic acid in water is very low (0.0017 g/100 g H_2O at 25°C) (52). Unfortunately, due to the high pH, the liquid will slowly capture carbon dioxide from the air, which can introduce an error by reducing the fluorescence yield (49).

The system was chosen over the earlier calcium benzoate solution, because of its enhanced sensitivity that is in part caused by structural reasons: there is only one possible chemical isomer (2-hydroxy-terephthalate anion, HTA) as the product of a single hydroxyl radical substitution on the highly symmetric terephthalate anion. Although the radiation-chemical yield for the hydroxy-terephthalate anion (HTA) product is about $G \approx 100$ nmol/J (about 16× less than for the Fricke dosimeter) high sensitivity is achieved because of its brilliant fluorescence, peaking at 420 nm when excited by 315 nm light (49). This allows the dosimeter system to be reasonably precisely capable of recording doses down to 5×10^{-3} Gy (49).

For low-LET radiation (60 Co gamma rays), the dosimeter displayed very good linearity between 0.03–8 Gy, with a mean error about ±6% when measuring in the low dose range of 0.03–1 Gy (48). Although it is possible to detect doses even below 0.01 Gy, the precision greatly decreases. The dosimeter has good postirradiation stability; no changes in fluorescence were observed over the period of multiple days or even weeks postirradiation, in contrast

with, e.g., the calcium benzoate fluorescence dosimeter (47, 48). Most important for the subject of the present study is that changing the dose rate 0.005–10 Gy/min resulted in no effects on the chemical yields of HTA (47).

Trimesic Acid Dosimeter

The studies of Matthews et al. (53, 54) show that the most sensitive fluorescence dosimeter, trimesic acid (TMA, benzene-1, 3, 5-tricarboxylic acid, $C_6H_3(COOH)_3$) was identified as a promising hydroxyl radical probe since it is also highly symmetric, like terephthalic acid, so it was thought to have only one product of hydrogen atom substitution by the hydroxyl radical. A very good linear fluorescence yield was found when irradiated by low-LET radiation (60 Co gamma rays) between 0.01– 10 Gy, while unirradiated fresh solutions have practically zero fluorescence. As opposed to the terephthalate dosimeter, the trimesic acid dosimeter was found to exhibit the highest radiation fluorescence yields in an acidic environment, having a sharp peak around solution pH = 2. Most of the studies were then performed at a recommended formulation of aerated solution of 10^{-3} M TMA in 0.01 M H_2SO_4 that exhibited good stability for at least 2 days postirradiation, less concentrated solutions of TMA suffered from postirradiation instability (53).

Although solutions of trimesic acid appear to provide, so far, the most sensitive fluorescence dosimeter, the species responsible for the fluorescence is not hydroxy-trimesic acid (HTMA) and has not been identified yet (54). This unfortunately means that absolute chemical yields of the dosimeter cannot be assigned and the product of irradiation cannot be compared against an equal reference. Fortunately, the excitation and emission maxima are 350 and 450 nm, respectively, nearly overlapping with the fluorescence maxima of acidified quinine sulfate (54), an available and popular fluorescence reference standard (55). When this combination of excitation and emission wavelengths was utilized, a dose of 10 Gy delivered by 60 Co gamma rays was approximately equivalent to the fluorescence of 0.8 μM quinine in 0.05 M sulfuric acid (allowing formulation of a provisional radiation-fluorescence yield $G_{FL} \approx 0.08$ μmol quinine/J), while unirradiated trimesic acid has practically zero fluorescence. The study of the effect of dose rate performed in the range of 0.03–10 Gy/min revealed a slight increase of fluorescence yield, amounting to about 4% per order of magnitude.

Coumarin-3-Carboxylic Acid Dosimeter

Coumarin ($C_9H_6O_2$, 2-H-chromen-2-one, 1-benzopyran-2-one) and its derivatives have been investigated extensively as $^{\bullet}OH$-sensitive fluorescence probes for the hydroxyl radical (56, 57), where the fluorescent species produced by hydroxylation is the 7-hydroxycoumarin (umbelliferone), among other derivatives hydroxylated to other positions. A derivative of coumarin, coumarin-3-carboxylic acid (C3CA, $C_{10}H_6O_4$) was selected as a better alternative to unsubstituted coumarin mainly due to the twofold enhanced fluorescence sensitivity of 7-hydroxy-coumarin-3-carboxylic acid (7-OH-C3CA) and the possibility of synthesis of other hydroxyl radical probes based on the specific properties of the carboxylic group (58, 59). Additionally, due to the carboxylic group, C3CA has better solubility in aqueous solutions (60) compared to unsubstituted coumarin (61). The utilization of C3CA for radiation chemical dosimetry has been the topic of a number of recent studies (32, 33, 60, 62–65). An advantage of this system, not shared by the trimesic acid system, is that the fluorescent product of irradiation is well known and commercially available and, hence, can be used for calibrations.

The 7-OH-C3CA molecule is fluorescent with an emission maximum at 450 nm and two excitation maxima at 350 and 395 nm, with the latter being more practical, because the C3CA ''mother'' molecule has an absorbance band that interferes with the 350 nm excitation maximum while also displaying a weak fluorescence emission (62), whereas when excited at 395 nm the C3CA molecule is practically non-fluorescent. Unfortunately, compared to the terephthalate and trimesic acid dosimeters the radiation-induced fluorescence yield of the C3CA dosimeter is about an order of magnitude weaker, primarily because of the relatively weak chemical yield of 7-OH-C3CA of only $G \approx 0.013$ μmol/J. This is primarily because only about 5% of the hydroxyl radicals end up substituting a hydrogen atom on the C3CA molecule on the C7 carbon position (66) and all the other hydroxyl derivatives (C4, C5, C6 and C8) that are created during radiolysis (67) are non-fluorescent (62).

Since the main application of dosimeter was intended for neutral biological solutions, in past studies the C3CA solutions were all buffered to achieve neutral pH between 6–8 (58, 68). As the value of pK_A for C3CA is 3.7 (69), it is assumed that in these conditions the molecule is fully deprotonated. Best results were achieved with inorganic phosphate buffer saline (PBS) at pH = 7.4, since using partially organic buffers has led to significantly reduced chemical yields (58). In the more recent studies of the C3CA dosimeter system (60, 62, 70, 71) in conditions that are more relevant to the present study, where time resolved measurements were performed via pulse radiolysis as well, the buffer utilized was an equimolar phosphate buffer (1:1 NaH_2PO_4/K_2HPO_4) with pH = 6.8. The reasons for choosing this buffer composition was that the mono- and dihydrogenphosphate anions have very low reaction rates with the hydroxyl radicals (70).

The C3CA dosimeter, even when at a concentration as low as 10^{-4} M C3CA, displays a constant yield for low LET photon radiation for doses up to 40 Gy, but above this dose the chemical yields start to decrease (68). The same kind of behavior was observed with 60 Co gamma rays on unsubstituted coumarin solutions, yet when the concentration of coumarin was increased to 10^{-3} mol/L the dosimeter

was capable of keeping linearity up to a dose of 420 Gy (57).

Specific research so as to the dose rate effect of low-LET radiation on the C3CA dosimeter has been shown by Collins et al. (68) with a pulsed 6 MV bremsstrahlung-linac source in the relatively small range of 0.8–4 Gy/min of average dose rate. The pulses were 4 μs long and had a maximum peak dose rate of 70 Gy/s [note: the value that the authors of (68) erroneously wrote is ''70 Gy/min'', given that the period between the pulses is several milliseconds long (72)]. Over the dose rate range for doses of a few tens of Gy the yield of the dosimeter decreased by up to 18% for unpurified reagent-grade C3CA compound, but only by about 2–4% when working with a C3CA purified by several recrystallization cycles (68). In the earlier studies performed by Ashawa et al. (57) on the non-carboxylated coumarin dosimeter, where the dose rate from a 60 Co gamma source was varied between 0.2 and 69 Gy/min, a threshold dose rate of 1 Gy/min (=0.017 Gy/s) was identified for solutions of 10^{-4} M coumarin, above which the yield started decreasing sharply by about 30% per order of dose rate magnitude.

Most recently, observations of the effects of dose rate on the yield of the C3CA dosimeter were published by Kusumoto et al. (73). High-energy-proton (27.5 MeV) irradiation was utilized in the dose rate range of 0.05–160 Gy/s and doses between 30 and 80 Gy were deposited. A substantial drop of the yield was observed, by over 60% in the dose rate range of 0.05–10 Gy/s. The authors have attributed this decrease to the effect of radiolytic oxygen depletion despite the relatively low doses utilized – see Discussion below for detailed analysis of this issue.

EXPERIMENTAL METHODS

Chemicals and Preparation of Solutions

The main compounds for the fluorescence dosimeter chemicals were purchased in solid crystalline form from the Sigma Aldrich company within 2 years prior to performing the experiments: quinine, trimesic acid (benzene-1, 3, 5-tricarboxylic acid), terephthalic acid (benzene-1, 4-dicarboxylic acid), coumarin-3-carboxylic acid (1-benzopyran-2-one-3-carboxylic acid) and 7-hydroxycoumarin-3-carboxylic acid (7-hydroxy-1-benzopyran-2-one-3-carboxylic acid). The ferrous sulfate compound used for the Fricke dosimeter was $(NH_4)_2FeSO_4.6H_2O$ and the compounds used for buffering the pH of the solutions, i.e., $NaH_2PO_4.2H_2O$, $Na_2HPO_4.2H_2O$, H_2SO_4, and NaOH were of ACS reagent grade or analytical grade (p.a.) from various suppliers. Water generated by an ELGA Classic class I ultrapure water filtration system (18.2 MΩ.cm) was used as the solvent.

The solutions were prepared by dissolving the solid crystals in water using magnetic stir-plates to prepare a stock and then diluting the aqueous stock into the final solution with the addition of the pH buffering agent (TA – sodium hydroxide, TMA – sulfuric acid, C3CA – phosphate buffer). For the trimesic acid (TMA) dosimeter, concentration of 10^{-3} M of TMA was selected instead of 10^{-4} M to avoid possible dose depletion effects, as indicated by Matthews et al. (54). Similar reasoning was used for the 10^{-3} M concentration of the C3CA dosimeter. For the terephthalate dosimeter the concentration of terephthalic acid was selected as 10^{-4} M, primarily to be comparable to the previously realized work, as studies have shown that the dosimeter can sustain good response linearity up to 30 Gy (49).

Fricke Dosimetry

Standard Fricke dosimetry was utilized to determine the dose rate of the custom irradiation positions in the 60 Co panoramic irradiator and in the dose-charge correlation experiments at the ELYSE electron beamline. A solution of 1 mM $(NH_4)_2FeSO_4.6H_2O$, 1 mM NaCl and 0.4 M H_2SO_4 was utilized. The radiation-induced change of absorbance ΔA in a 1-cm pathlength cuvette for the absorption maximum of Fe^{3+} at 304 nm was measured and the dose was calculated as $D = \Delta A \times 287$ Gy, based on temperature and density corrections recommended in ref. (22) (both irradiation and analysis temperature was near 21°C). A Varian Cary 5000 instrument was used for the spectrophotometric measurements of Fricke dosimeter samples that were irradiated in glass vials and then transferred into PMMA cuvettes for the absorption measurements.

60 Co Gamma-Ray Irradiator

The IL60PL 60 Co gamma ray operated by the Institute of Chemical Physics (ICP) of Université Paris-Saclay in Orsay, France, was utilized for reference irradiations of the chemical dosimeters. The source uses a panoramic configuration with two aluminum tables with marked positions on a 50 mm grid and the irradiation room is big enough that by selection of distance dose rates from ~0.5 Gy/h up to a ~7 kGy/h were achievable. The majority of the samples utilized for the studies of the fluorescence dosimeters were irradiated at a special position from the source, at a low dose rate of 6.85 Gy/h (1.90 mGy/s to achieve high precision of the target doses for the sensitive fluorescence dosimeters that were to cover a range of doses below 3 Gy. The dose rate was determined by Fricke dosimetry in the same type of vials and geometry as the fluorescent dosimeters (see below).

The ELYSE Accelerator

The ICP also operates a radiofrequency linear accelerator (LINAC) called ELYSE with a UV laser-triggered photocathode capable of producing electron pulses with picosecond pulse length. The electron energies can be varied between 4–9 MeV and the charge of the electron pulse can be varied between 0.1–6 nC. For the experiments, the

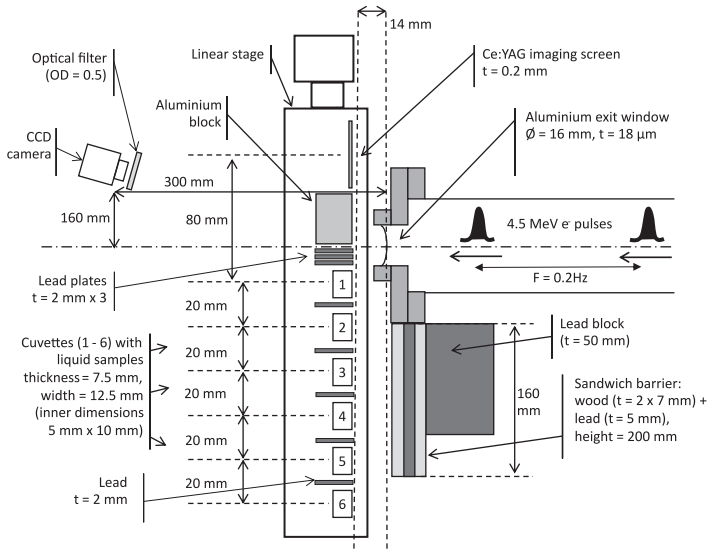

FIG. 1. Irradiation setup at the outlet of the ELYSE accelerator

selected electron energy was 4.5 MeV and the electron pulse charges were varied between 0.2 and 3 nC. The pulse length (which was qualitatively an important parameter for the goal of this work) can be as short as 4 picoseconds, and is synchronized with probing light pulses from a femtosecond laser (74, 75). The charge of the electron pulse is measured by an in-vacuum Faraday cup that serves a second purpose as a beam blocker.

The ELYSE accelerator is usually utilized for investigations of rapid processes via pulse radiolysis, so certain improvised modifications of the irradiation area had to be done to facilitate the characterization of chemical yields of liquid chemical dosimeters. In total, about 10–15 workdays of ELYSE beamtime were utilized for the experiments described in this study.

Irradiation Setup at ELYSE

The irradiation setup is shown in Fig. 1. The liquid samples of the solutions of chemical dosimeters were irradiated in quartz cuvettes with walls 1.25 mm thick, a 5 mm liquid optical path, and a 10 mm wide liquid compartment to have a well-defined geometry of the liquid pathlength of the penetrating fast electrons. The cuvettes were filled by 1.50 cm^3 of solution, so the approximate height of the liquid solution in the cuvette was about 30 mm, the top of the solution was formed into a meniscus due to surface tension. The liquid was transferred from a stock bottle to the cuvettes approximately 30–60 min prior to irradiation. After irradiation, the liquid was transferred to plastic cuvettes for storage and fluorescence measurement (see below).

Imaging of the electron beam by Cherenkov light (75), as well as Monte Carlo simulations by the EGS code (75, 76) indicated that in such geometry only very few electrons should scatter out of the lateral sides of the cuvette, so it was assumed that nearly every 4.5 MeV electron that entered through the front cuvette window should also have left via the back of the cuvette.

The accelerator had to be powered down to allow presence of personnel in the experimental hall, so multiple samples were mounted on a remotely controlled translation stage to allow for irradiating multiple samples in a fast sequence. The electron beam profile (quality of the electron beam focus) was adjusted through monitoring by a CCD camera (Sony XC-ES50, equipped with a Fujinon HF25HA-1B 1:1.4/25 mm objective) that was looking at fluorescence induced by the electron beam in a 0.2 mm thick Ce:YAG radiofluorescent screen that was also mounted on the same remote-controlled translation stage as the liquid samples intended for irradiations.

Changing the amount of charge in the electric pulse involved resetting the femtosecond laser pulse energy and some of the parameters of the LINAC - this usually required the realignment and re-focusing of the electron beam to achieve optimum focus and ensure that most of the pulse charge was injected into the irradiated quartz cuvette. However, at any single charge setting a whole row of samples were used; therefore, the focusing conditions were the same for the same set of samples (dose).

The procedure for irradiating the sample for each particular value of the electron pulse charge (dose) was as follows: First, the Ce:YAG screen was moved into position and the accelerator was operated at a higher repetition rate (usually 5 Hz). During this period, the beam focus was adjusted to maximize the number of electrons from each pulse to hit the center of a 10×10 mm digital targeting rectangle on the Ce:YAG screen that was pre-aligned with the position of the liquid inside the quartz cuvettes. Due to the high frequency, many thousands of pulses passed through the Ce:YAG screen during the beam alignment procedure; hence, radiation shielding in the form of a lead

TABLE 1
Composition of Solutions Prepared for the Experiments and Chosen Spectrofluorimetric Parameters

Solution/dosimeter	Composition of aqueous solutions	Excitation range (>50% maximum)	Selected excitation wavelength(s)	emission range	Selected emission wavelength
Terephthalate dosimeter	0.1 mM TA, 0.4 mM NaOH	293-328 nm	315 nm	400-480 nm	425 nm
Trimesic acid dosimeter	1 mM TMA, 0.01 M H_2SO_4	320-370 nm	345 nm	425-500 nm	450 nm
Quinine reference	0.25-1 μM quinine, 0.01 M H_2SO_4	300-370 nm	315 nm (TA), 345 nm (TMA)	420-500 nm	450 nm
C3CA dosimeter	1 mM C3CA, 0.01 M PB	355-420 nm	395 nm	430-475 nm	442 nm
7-OH-C3CA reference	0.25-1 μM 7-OH-C3CA, 0.01 M PB	355-420 nm	395 nm	430-475 nm	442 nm
Fricke dosimeter	1 mM $(NH_4)_2FeSO_4$, 1 mM NaCl, 0.4 M H_2SO_4	-	*absorbance,* 304 nm	-	-

Abbreviations: C3CA = coumarin-3-carboxylic acid; 7-OH-C3CA = 7-hydroxy-coumarin-3-carboxylic acid; TA = terephthalic acid; TMA = trimesic acid; PB = phosphate buffer (1:1 molar mixture Na_2HPO_4 + NaH_2PO_4 at pH = 6.8).

brick, several lead plates and of an aluminum block was added to protect the sensitive fluorescence dosimeter samples from scattered radiation that would cause them to receive dose before their proper irradiation (see Fig. 1). After the alignment was completed, the accelerator frequency was reduced to 0.2 Hz, this allowed for enough time between the pulses to slide a beam blocker inside the vacuum tube in and out of the beam between each pulse, and, hence, make it possible to expose each cuvette with a fluorescence dosimeter (TA, TMA, C3CA) to exactly one electron pulse. The samples of Fricke dosimeter were irradiated by 10 pulses to offset the issue of the low sensitivity (see further discussion below).

Fluorescence Measurements

The fluorescence of the liquid samples was measured off-line no sooner than 1 h and no later than 8 h postirradiation by either the 60 Co gamma irradiator or the ELYSE electron accelerator.

The dosimeters were irradiated in rectangular quartz 5-mm path-length optical cuvettes on the electron beamline and in round 5 mL screwcap borosilicate glass vials in the 60 Co panoramic irradiator. After expsoure, the liquid samples were transferred to standard 1-cm fluorometric optical cuvettes made from polymethylmethacrylate (PMMA; Kartell, Italy), that had no appreciable UV-Vis absorption above 280 nm where excitation and emission wavelengths were utilized for the spectrofluorometric measurements. During trial irradiations in these PMMA cuvettes the fluorescence induced by 60 Co irradiation of the dosimeters revealed no difference between irradiation in glass vials and plastic cuvettes aside from occasional (<3%) incidence of large outlier results.

The spectra were measured in a Fluorolog-3 (Jobin-Yvon) spectrofluorometer in a temperature stabilized cuvette holder (25°C) using a photomultiplier detector (Hamamatsu R2658P) temperature stabilized in a cooled enclosure (Amherst Scientific, Inc.). The selected excitation and emission wavelengths utilized for each dosimeter system are indicated in Table 1. Detailed explanation for these measurement settings is contained in the Supplementary Information (https://doi.org/10.1667/RADE-20-00292.1.S1), along with examples of excitation and emission spectra and a description of how the fluorescent signals were normalized using solutions of reference standards.

RESULTS

Determination of Doses Delivered by Pulses from the ELYSE Accelerator

To determine the absorbed energy in the sample we have exploited the capabilities of the *Geant*4 Monte Carlo simulation toolkit software (77). The geometry of the irradiation setup was replicated *in silico* with material definitions taken from the NIST database via the G4Nist-Manager class. Energy cut-off was set to 50 eV. Figure 2 shows 300 simulated electron tracks; electrons are arriving from the left through 18-μm aluminum foil and 14 mm of air, and then penetrating 1.25 mm of a quartz (SiO_2) cuvette wall to reach the 5-mm thick aqueous sample (Fricke dosimeter). In Fig. 3 the distribution of absorbed energy in consecutive 50-μm thick layers is shown as a result of simulation of propagation of 10^6 electrons in the liquid sample; notable are two build-up regions near the quartz cuvette walls. The deposited energy linearly increases towards the back of the cuvette; the difference between the energies absorbed at the back and at the front of the cuvette sample compartment is about 14%.

From the dependence of the absorbed energy in the liquid sample as a function of the charge of the primary electrons in the pulse a value of 1.16×10^{-3} J/nC was obtained. This value was further used for the conversion of the Faraday cup readings in nanocoulombs to absorbed dose in the liquid sample in Gy, assuming the mass of the Fricke dosimeter to be 1.536 g.

The pulse charges were varied from zero up to a maximum of 3.0 nC, which would then translate to a maximum dose of 2.26 Gy, averaged over the liquid volume of the cuvette. However, most of the dose was delivered within a diameter of 6 mm, so only a small part of the solution was subjected to the focus of the electron beam

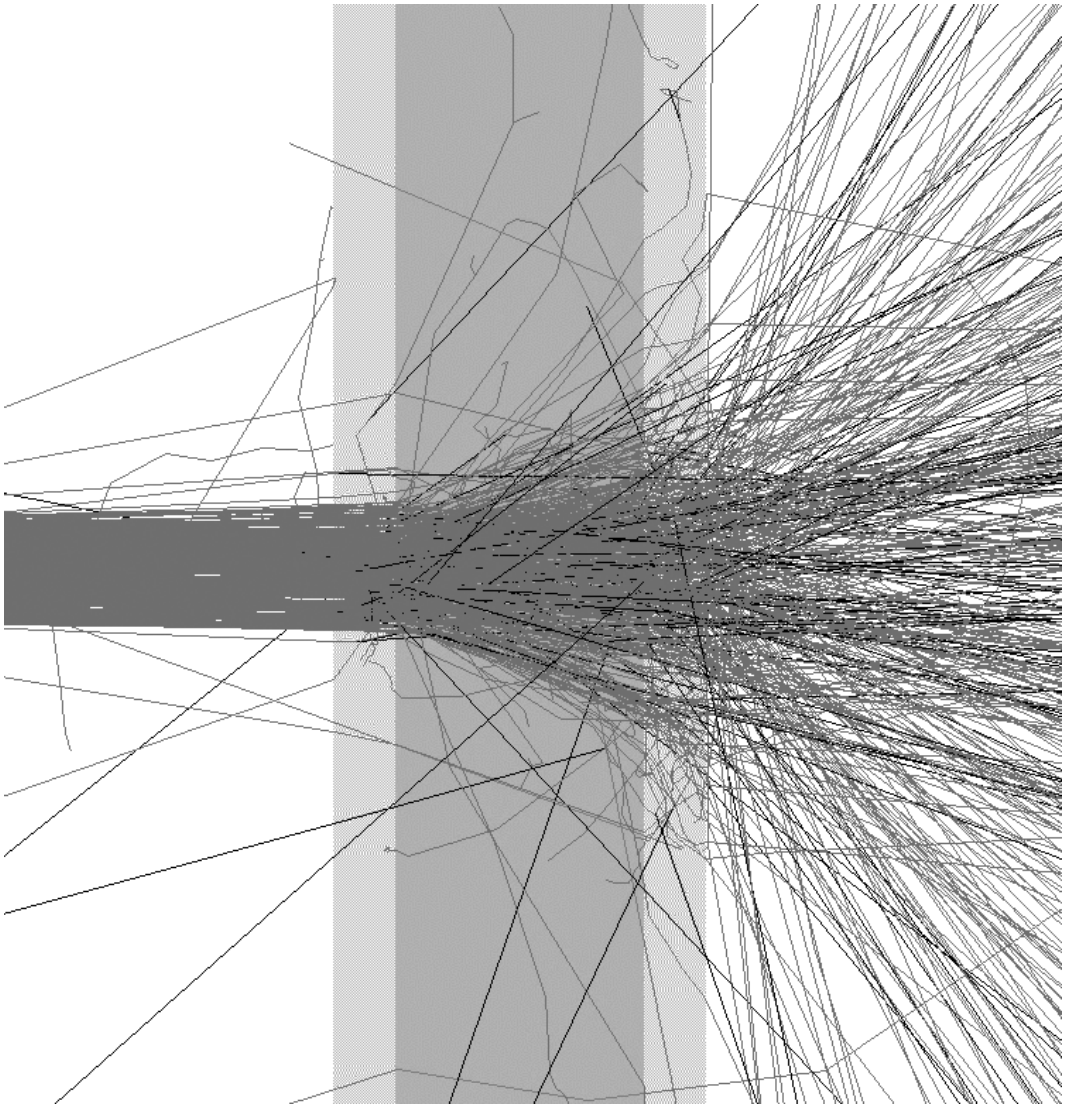

FIG. 2. Simulation of 300 tracks of 4.5-MeV electrons propagating in air from the left into a cuvette with 1.25-mm thick quartz walls filled with a 5-mm thick layer of Fricke dosimeter; gray tracks: electrons, black tracks: photons.

(focus area of ~30 mm^2 vs. ~300 mm^2 of the sample), hence, the estimate of the peak dose at which the majority of the radiation energy was translated to the sample is about ~20 Gy. Given the 4–6 ps length of the electron pulse, at such peak doses the dose rate reaches the order of teragrays/s (TGy/s = 10^{12} Gy/s).

Unfortunately, it was discovered through initial liquid dosimetric experiments that at higher pulse charges (>1.5 nC) the doses were not proportional to the delivered charge. This was most likely caused by Coulomb repulsion, which was making it harder to focus all the charge into the desired location of the sample cuvette.

To characterize the effect, images of the intensity of fluorescence induced by the beam on the Ce:YAG screen were recorded; with room lights switched off (see Fig. 4). The images were captured by the monochrome CCD camera operating at a shutter speed of 1/100 s when the accelerator was operated at the elevated frequency of 5–10 Hz. Care was taken to ensure equal capture conditions for each charge setting. A fixed neutral optical density filter was placed in front of the CCD camera (see Fig. 1) with its optical density value (OD = 0.5) selected to enable maximum sensitivity at the lowest charge settings while preventing oversaturation of the signal at the highest charge setting. Subsequently, the images of an area that matched the liquid sample in the cuvette were processed and analyzed by ImageJ (78) and in a spreadsheet program to compare the fluorescence intensities induced by each shot. Correlation of radio-fluorescence intensities confirmed the issue of non-linearity of the dose delivered into the target area (Fig. 5).

The Faraday cup was located about 500 mm ahead of the sample, although the cup did measure the total pulse charge emitted by the accelerating cavity, the poorer focusing

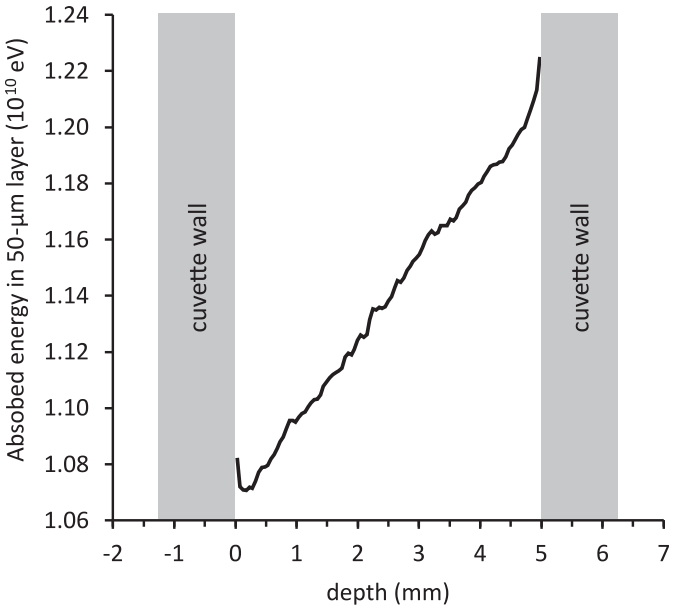

FIG. 3. Distribution of the absorbed energy from initially 4.5-MeV electrons in 50 µm liquid dosimeter layers stacked along the beam propagation. Notable are the two build-up regions near the cuvette walls. Simulation of 10^6 electrons. Beam is arriving from the left.

capability at higher pulse charge settings resulted in a minor part of the charge being diverted to trajectories that collided with the walls of the exit tube of the accelerator. This is partly evidenced by the weak, yet visible, circular shape of the radio-luminescence that approximates the projection of the 16-mm wide-exit window of the accelerator system on the Ce:YAG screen (Fig. 6). Importantly, integrating the luminescence across the whole 16 mm diameter corresponding to the projection of the exit port of the accelerator (Fig. 6) did not change the outcome of the analysis, this supports the assumption that at high charges some of the electrons were deflected onto trajectories that collided with the beam transport tube.

The intensity of the radiation-induced luminescence in the Ce:YAG screen was assumed to be linearly proportional to

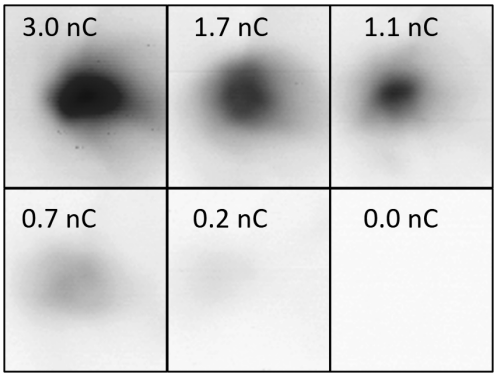

FIG. 4. CCD images (negatives) of the Ce:YAG screen luminescence visualizing the profiles of the electron pulses in the position of the 1-cm wide cuvette entry window with inscribed corresponding values of pulse charges measured by the Faraday cup

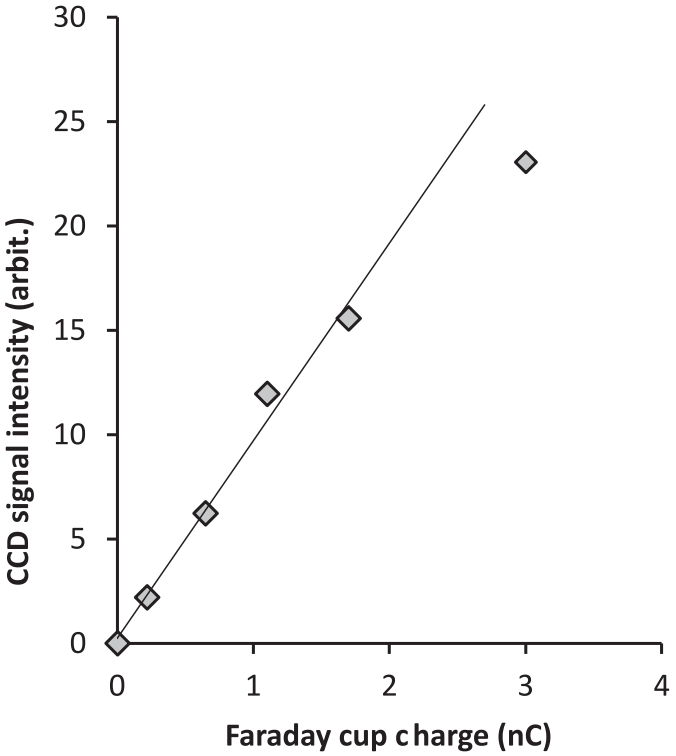

FIG. 5. Example of the plot of intensity of prompt radio-fluorescence of the Ce:YAG screen induced in the focus of the electron beam as recorded by the CCD camera correlated against the pulse charge measured by the Faraday cup. A linear trendline is plotted through the first five datapoints to indicate the significant nonlinear effect at the highest charge setting.

the number of incident electrons (pulse charge) in the beam, regardless of the utilized charge intensity. The maximum charge utilized in the pulses was 3 nC and it was focused at best into an area of roughly 5×5 mm $= 0.25$ cm^2, leading to

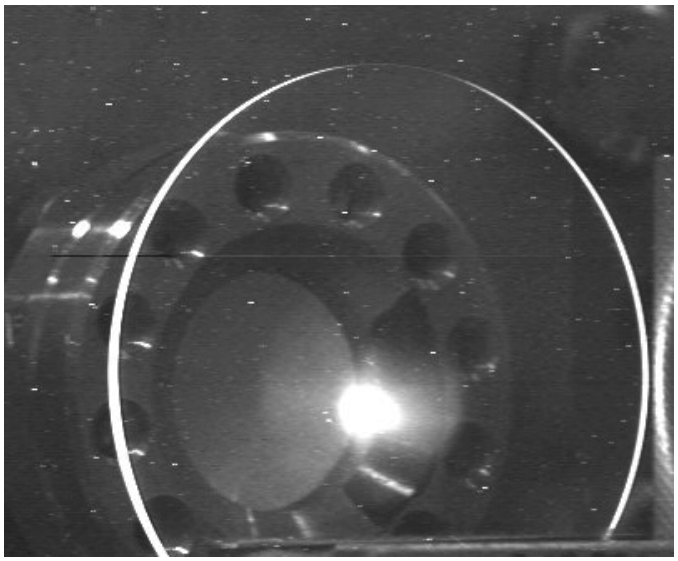

FIG. 6. Image of the beam exit port and the radio-fluorescence produced by the interaction of the electron beam with a 0.2 mm thick Ce:YAG imaging screen (room lights lit).

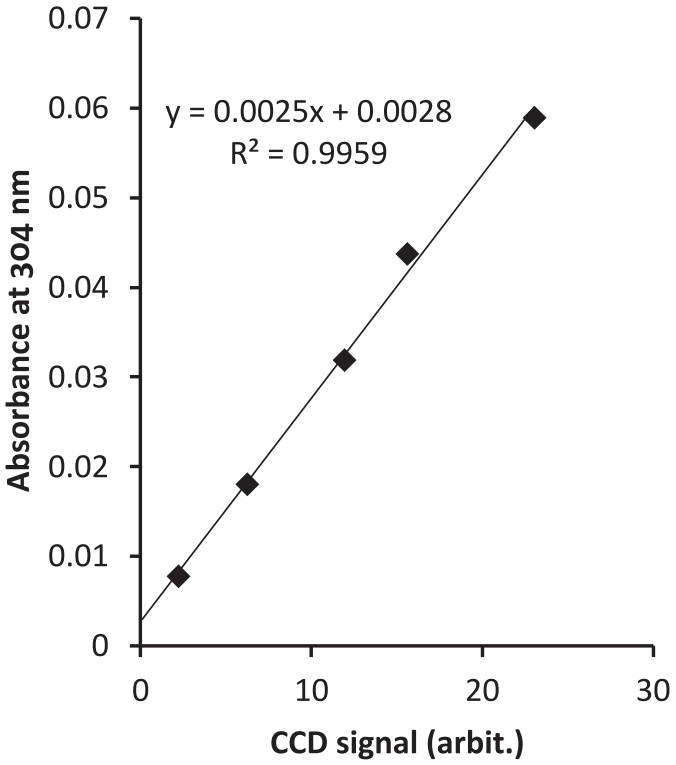

FIG. 7. Example of the correlation of the absorbance of Fricke dosimeter solutions (1 cm cuvettes) induced by 10 identical electron pulses vs. the signal of the intensity of the prompt radio-fluorescence by the Ce:YAG screen as recorded by the CCD camera

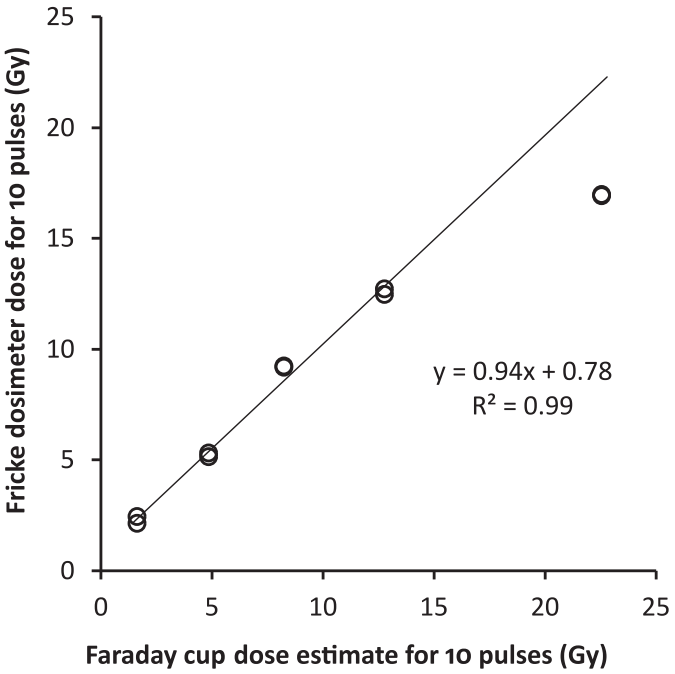

FIG. 8. Correlation of dose estimates calculated from the charge accumulated from 10 electron pulses as measured by the Faraday cup with the dose as measured by the Fricke dosimeter (baseline corrected)

a maximum charge area density of 12 nC/cm^2 and to an expected energy density of 2.7×10^{18} eV/cm^3, given the stopping power of the Ce:YAG crystal for fast electrons of 6.7 MeV/cm (79), i.e., at least 2 orders below the intensities that were reported to start providing nonlinear/saturation results from the Ce:YAG radio-luminescent screen [30 μC/cm^2 (80); 2×10^{20} eV/cm^3 = 32 J/cm^3 (81)].

Due to the issue of low reliability of calculation of the dose by measuring pulse charges by the Faraday cup, it was decided to irradiate samples of Fricke dosimeter solutions along with the three fluorescence dosimeters. Unfortunately, the Fricke dosimeter sensitivity is too low to accurately determine doses below 1 Gy, so it was decided to irradiate each Fricke dosimeter sample with exactly 10 pulses. It was assumed that the measurements using repeated irradiation would produce acceptable results, because of the long period between each pulse (5 s), which should have been sufficient for the majority of chemical reactions to be complete, and because the doses from each pulse were still too low to cause measurable interactions with the radiolytic products from previous pulses.

When plotted against the CCD signal intensity (Fig. 7), instead of against the Faraday cup charge measurements, the absorbance of the Fricke dosimeter solutions, measured in 1-cm pathlength cuvettes, followed a near-perfect linear dependence, free from the nonlinearity at the high charge level that could be observed in Fig. 5.

The absorbances measured in the Fricke dosimeter solutions (in absorbance units = AU) were converted into dose using coefficient 287 Gy.cm/AU (22), and the doses were then plotted in Fig. 8 against the dose estimates calculated from the charge measured by the Faraday cup using the coefficient 1.16×10^{-3} J/nC calculated by Geant4 simulations (see above).

As can be seen in Fig. 8, in the region of linear proportionality, the doses determined by the method of Fricke dosimetry are close to unit proportionality with the doses estimated from pulse charge measurements using the Monte Carlo calculations. Consequently, it seems reasonable to assume that the Fricke dosimeter does not experience a reduced chemical yield under the parameters of the experiment (peak doses below 20 Gy, pulse length over $\sim 5 \times 10^{-12}$ s). However, this is in contrast with the expectations one would base on the results of previous studies (18) that indicate that at the dose rates above 10^6 Gy/s the yields of the Fricke dosimeter should drop by almost twofold; this disparity will be discussed below.

It is important to note that the dose estimates based on pulse charge measurements represent the higher bound of the dose delivered to the samples and, in the linear portion of the plotted date in Fig. 8, the Fricke dosimeter results are in good agreement with this higher bound. In combination with the proportionality of the Fricke data to the CCD signal intensity (Fig. 7), the doses determined by Fricke dosimetry are assumed to be the best estimates of the absorbed dose in the specific liquid sample geometry utilized in this study. Hence, the yields of the fluorescence dosimeters in this

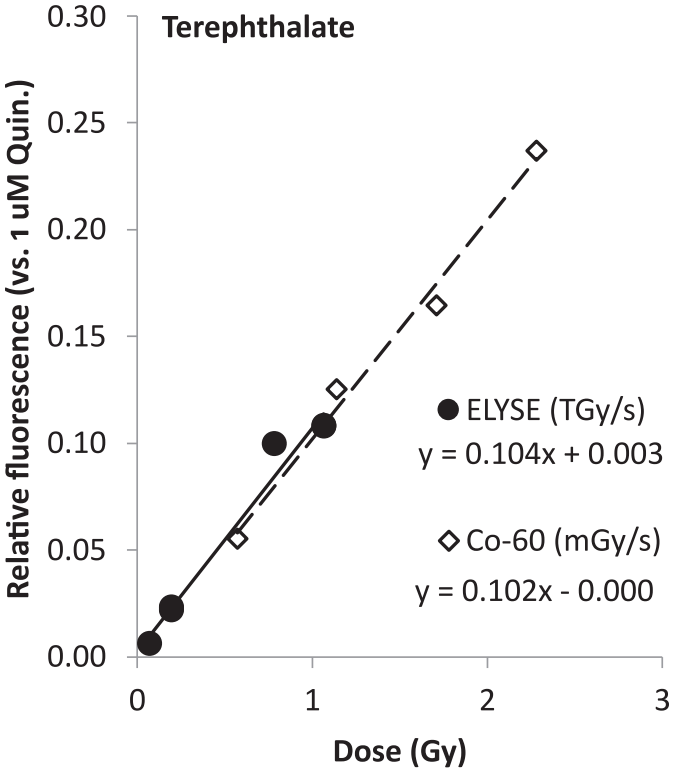

FIG. 9. Comparison of the fluorescence of liquid samples of the terephthalate dosimeter (0.1 mM terephthalic acid in 0.4 mM NaOH) caused by irradiation with picosecond electrons from ELYSE and with 60 Co gamma-ray source; the dose was determined by Fricke dosimetry (see text); the liquid fluorescence measurement was normalized against the fluorescence of solutions of 1 μM quinine in 0.4 M H_2SO_4 (for more details see Supplementary Information; https://doi.org/10.1667/RADE-20-00292.1.S1).

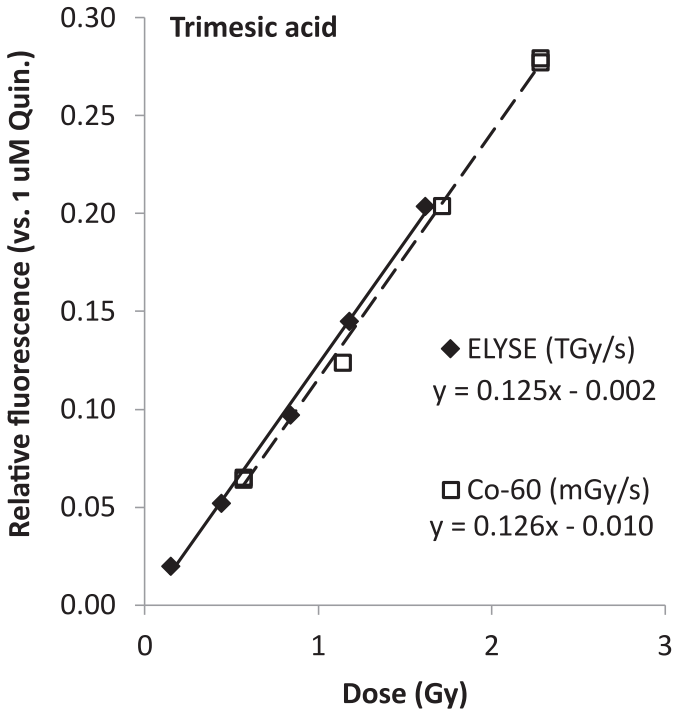

FIG. 10. Comparison of the fluorescence of liquid samples of the trimesic acid dosimeter (1 mM trimesic acid in 0.01 M H_2SO_4) caused by irradiation with picosecond electrons from ELYSE and with 60 Co gamma-ray source; the dose was determined by Fricke dosimetry (see text); the liquid fluorescence measurement was normalized using solutions of 1 μM quinine in 0.4 M H_2SO_4 (for more details see Supplementary Information; https://doi.org/10.1667/RADE-20-00292.1.S1).

study were then calculated relative to the doses determined by Fricke dosimetry.

Dose Rate Effects on the Chemical Yields of the Fluorescence Dosimeters

As a result of previous considerations, it seems most reasonable to evaluate the yields of the fluorescence dosimeters irradiated by ELYSE from plots correlating their fluorescence against the doses determined by the Fricke dosimeter, instead of against the doses calculated from the pulse charges measured by the Faraday cup. These plots are then compared to equivalent plots determined by standard 60 Co gamma-ray irradiation.

The results of the experiments are summarized in Table 2. The fluorescence yields at different dose rates for equivalent doses appear identical for the fluorescent dosimeters based on aqueous solutions of terephthalic acid and trimesic acid (see Figs. 9 and 10), while they differ substantially for the solutions of coumarin-3-carboxylic acid (Fig. 11), where the fluorescence yield drops by about 60% for the ultrafast pulsed irradiation.

TABLE 2
Comparison of the Effect of Elevated Dose Rate from the Pulsed Source (ELYSE) and a Continuous 60 Cobalt Gamma-Ray Source on the Fluorescence Yields of Three Different Dosimeters

	Radiolytic yields of fluorescence dosimeters (fluorescence relative to 1 μM standard/Gy**)		
Dosimeter system	**60 Co (mGy/s)**	**ELYSE (TGy/s)**	Relative yield change mGy/s → TGy/s
Terephthalate	**0.102** ± 0.008*	**0.104** ± 0.007*	(+ 2 ± 11) %
Trimesic acid	**0.126** ± 0.003*	**0.125** ± 0.005*	(+ 0 ± 5) %
C3CA	**0.0168** ± 0.0003*	**0.0065** ± 0.0002*	(− 61 ± 4) %

* Standard error of regression slope.
** Dose determined by Fricke dosimetry (see text).

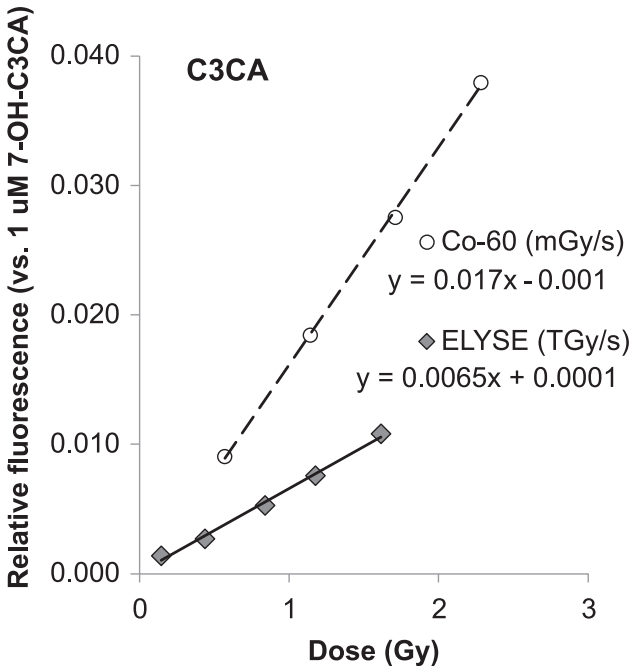

FIG. 11. Comparison of the fluorescence of liquid samples of the coumarin-3-carboxylic acid dosimeter (C3CA in 10 mM phosphate buffer at pH = 6.8) dosimeter caused by irradiation with picosecond electron pulses from ELYSE and with 60 Co gamma-ray source; the dose was determined by Fricke dosimetry (see text); the liquid fluorescence measurement was normalized against the fluorescence of solutions of 1 μM 7-OH-C3CA in 10 mM PB of pH = 6.8 (for more details see Supplementary Information; https://doi.org/10.1667/RADE-20-00292.1.S1).

DISCUSSION

The acquired experimental results of the study revealed two interesting facts about the effect of low-dose pulses administered under very high dose rate: 1. the yield of the Fricke dosimeter appears to be unreduced, 2. out of the three fluorescence dosimeters only the C3CA system shows a significant drop in its yield.

Unchanged High Dose Rate Yields of the Fricke Dosimeter

Even though previous studies (16–18) of the Fricke dosimeter system indicate that chemical yields should significantly decrease at dose rates much higher than 10^6 Gy/s, the present results indicate that for pulsed radiation no such phenomenon can be observed for dose rates even a million-fold higher when small doses per pulse (i.e., less than 10 Gy/pulse) are administered over the duration of multiple seconds and the total average dose does not exceed 20 Gy. As mentioned previously, this is in line with the findings of Rotblat and Sutton (15) that the greatly decreased yields at high dose rates were likely a result of high peak doses (>400 Gy) in the radiation pulses due to a change of chemistry caused by depletion of oxygen. The expected reason is that the conversion of the reducing species (e_{aq}, $H^\bullet$) into hydroperoxyl radicals $HO_2^\bullet$ that act as oxidizers toward Fe^{2+} is suppressed under anoxic conditions – this then results in a drop of Fe^{3+} yields (15, 20). However, as has been mentioned in the introduction above, a minor decrease of yield was observed for dose rates and total doses that could not be explained by the effect of oxygen depletion (15, 17, 20). This decrease is thought (15, 20) to be likely caused by radical-radical reactions. In fact, with high dose per pulse the overlapping between spurs occur at shorter time than 200 ns, therefore, the radical-radical reactions occurs before reactions between the radicals and solutes in homogenous step (82). This was already observed directly by pulse radiolysis and analyzed for the system of Fricke dosimeter by computer modeling (82, 83) that confirmed Fe^{3+} yield decrease as a result of elevating the pulse dose rather than by shortening the pulse. Since the rate of radical-radical reactions is proportional to the square of concentration, they should become more significant when the dose rate is increased by raising the amount of dose per pulse rather than by making the pulses shorter, at least when the pulse length is shorter than the characteristic lifetime for such reactions.

In the performed experiments in this study the highest peak dose was of the order of 10^1 Gy, so assuming an average energy deposited in a spur to be 60 eV (84) the concentration of spurs would be about 10^{18} $dm^{-3} = 10^3$ μm^{-3}, giving an estimate of mean spur distance of $x \approx 100$ nm. For the primary reactive species with their diffusion coefficients D in the range of (3–7) $\times$ 10^9 nm^2/s (85) the overlap with species produced from a neighboring spur should not take place until about a mean diffusion time $t = x^2/6D \approx 10^{-7}$ s. As a result, increasing the dose rate value by making the pulses shorter than about $\sim 10^{-7}$ s at a constant dose of $\sim 10^1$ Gy should not affect the chemical yields. This could explain that the relatively low doses (<10 Gy) that were delivered by the ELYSE accelerator have not resulted in recognizable decrease of the radiation chemical yield of Fe^{3+} in the Fricke dosimeter solutions despite the formally very high dose rates at which they were administered.

A deeper look into the important reactions involved in the radiation-chemical mechanism of the Fricke dosimeter indicates that the dose-sensitive radical-radical reaction that is responsible for the decreasing yields of the Fricke dosimeter (at doses that are well below the oxygen depletion effect) is most likely the reaction of $HO_2^\bullet$ with $^\bullet OH$ during the first 10 μs of the reaction.

Modeling based on rate constants from Bielski et al. (86) and Ershov et al. (87) indicates that the following two reactions are competing for the $OH^\bullet$ radical:

$$OH^\bullet + Fe^{2+} \rightarrow OH^- + Fe^{3+}; k_1 = 3.2 \times 10^8 M^{-1} s^{-1} (86), \quad \text{(R1)}$$

$$OH^\bullet + HO_2^\bullet \rightarrow H_2O + O_2; k_2 = 7.1 \times 10^9 M^{-1} s^{-1} (87). \quad \text{(R2)}$$

In the strongly acidic solution, all solvated electrons are rapidly scavenged by hydrogen ions ($[H^+] \approx 0.4$ M) and

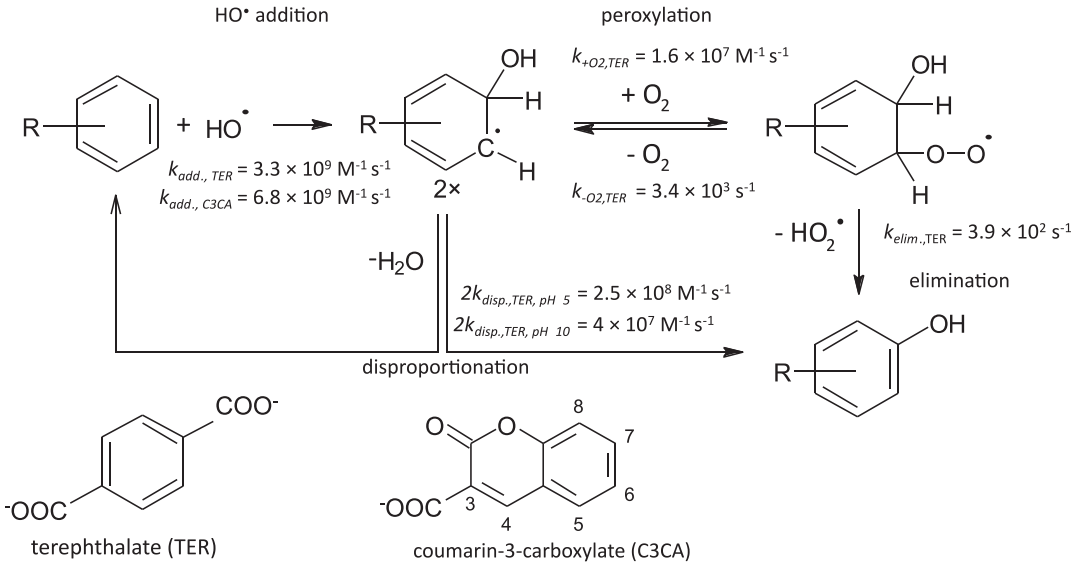

FIG. 12. Reaction scheme responsible for radiolytic production of OH-substituted products in the schemes of the terephthalate and the C3CA dosimeter. Experimentally established rate constant values are from Fang et al. (42) for the terephthalate system (TER) and from Yamashita et al. (60) for the addition reaction in the C3CA system.

form hydrogen atoms [$\tau \approx 10^{-10}$ s for $k = 2.3\times10^{10}$ $M^{-1}s^{-1}$ (87)]. The hydroperoxyl radical $HO_2^\bullet$ is then formed by the reaction of hydrogen atoms with the dissolved oxygen molecules [$[O_2] \approx 3 \times 10^{-4}$ M (88)]:

$$H^\bullet + O_2 \rightarrow HO_2^\bullet; k_3 = 2.0 \times 10^{10} M^{-1}s^{-1} (87). \quad (R3)$$

Originally, Rotblat and Sutton (15) have speculated [in the absence of rate constant data for reaction (R3)] that the reaction responsible for the decrease of the yield in these conditions was the recombination of $H^\bullet$ with the $OH^\bullet$ radical:

$$H^\bullet + OH^\bullet \rightarrow H_2O; k_4 = 7.0 \times 10^9 M^{-1}s^{-1} (87), \quad (R4)$$

However, with present day's knowledge (87), it can be easily shown that in the presence of dissolved oxygen, reaction (R3) would consume all $H^\bullet$ much sooner ($H^\bullet$ lifetime estimate, $\tau_{H,\ 3} \approx 10^{-7}$ s) than reaction R4 could take place [$\tau_{H,\ 4} = \tau_{OH,\ 4} \approx 10^{-4}$ s, assuming $[OH^\bullet]_{1\ ns} \approx [H^\bullet]_{1\ ns} \approx 3 \times 10^{-6}$ M for the 10 Gy dose (87)]. In addition, since k_3 is almost 100-fold greater than k_1, reaction (R3) is mostly completed before the $OH^\bullet$ start to be scavenged by the Fe^{2+} ions ($\tau_{OH,\ 1} \approx 3 \times 10^{-6}$ s, for 1 mM Fe^{2+}), in spite of the unfavorable ratio of Fe^{2+} and O_2 concentrations $[Fe^{2+}]:[O_2] \geq 3$.

The concentration of the newly formed $HO_2^\bullet$ is partially consumed in reaction R2 by the available $OH^\bullet$ radicals ($\tau_{OH,\ 2} \approx \tau_{HO2,\ 2} \approx 10^{-4}$ s for 10 Gy, $\tau_{HO2,\ 2} \approx 10^{-5}$ s for 100 Gy), even if the $OH^\bullet$ concentration is ultimately suppressed by reaction R1. The relatively minor contribution of reaction R2 on the $OH^\bullet$ radicals is magnified in significance, because the combined loss of 1 pair of $HO_2^\bullet$ and $OH^\bullet$ results in a net decrease of the yield by 4 Fe^{3+} ions in the multi-step mechanism of the Fricke dosimeter (15).

Reduced High Dose Rate Yields of the C3CA Dosimeter

Out of the three fluorescence dosimeters, only one displays a significant dose rate effect – the C3CA dosimeter. This is partially surprising, since the C3CA dosimeter shares at least with the terephthalate dosimeter the same principal reaction mechanism that produces the fluorescent compounds: substitution of a hydrogen atom attached to the main aromatic ring by a hydroxyl group (unfortunately, in the case of the trimesic acid dosimeter the reaction product and the underlying chemical mechanism are unknown). Nonetheless, as mentioned above, the recent study by Kusumoto et al. (73) does reveal that for low-LET radiation the dosimeter exhibits dropping yields already when raising the dose rate above 0.05 Gy/s, which is an effect that has not been observed for neither the terephthalate nor the trimesic acid dosimeter. Kusumoto et al. (73) interpret their results through the mechanism of oxygen depletion; however, this appears to be unlikely given the doses administered in their study were in the range 30–80 Gy, well below the ~500 Gy dose at which oxygen depletion effects usually manifest in aerated aqueous solutions (15, 20, 89). The authors considered as unlikely the hypothesis that the yield drops were caused by radical-radical interactions, but in their analysis, they focused on proving that these would need to take place in the early stages ($<10^{-5}$ s) of the radiation chemical process as a result of track overlaps. However, the mechanism of the C3CA dosimeter involves the presence of radicals that have significant lifetimes ($>10^{-3}$ s), which explains the reduced yields based on radical-radical reactions in the later stages.

Figure 12 shows the scheme of the proposed reaction mechanism responsible for the radiolytic production of OH-substituted products in the schemes of the terephthalate and

the C3CA dosimeter. The scheme is based on the investigation of the terephthalate system by Fang et al. (42), later proposed by Louit et al. to be applicable in both unsubstituted (67) and substituted (60, 62, 73) coumarin systems.

In the aerated form, the main channel of the reaction mechanism that leads to the formation of fluorescent hydroxy-substituted species for both the terephthalate and the C3CA dosimeters is assumed to consist of three main steps, involving the reaction of intermediate states with molecular oxygen, dissolved in the aqueous solutions (42, 60, 62, 67, 90). The value of the rate constant of the initial ''scavenging'' reaction step of the aromatic compounds towards the hydroxyl radical has been found to be approximately 5×10^9 M^{-1} s^1 (91) and is expected to produce a reactive adduct (hydroxy-dienyl radical, symbolized in the following text as HO-$R^\bullet$), shown as the first product in Fig. 12).

The $OH^\bullet$ addition to the aromatic compounds is complete by 10^{-5} s (lifetime estimates are $\tau_{add,\ C3CA} \approx k_{add,\ C3CA}^{-1} \bullet [C3CA]^{-1} \approx 150$ ns and $\tau_{add,\ TER} \approx k_{add,\ TER}^{-1} \bullet [TER]^{-1} \approx 3$ μs, assuming $[C3CA] = 10^{-3}$ M and $[TER] = 10^{-4}$ M). In the presence of O_2, the next step in the reaction scheme (Fig. 12) is a somewhat slower peroxylation reaction of the adduct with dissolved molecular oxygen, leading to formation of a hydroxy-dien-peroxyl radical (HO-$RO_2^\bullet$) and then, in the third step, to elimination of a hydroperoxyl radical, $HO_2^\bullet$, with the stable product being the hydroxylated aromatic molecule.

So far, the most thorough investigation of the reaction mechanism of the C3CA dosimeter system has been performed by Yamashita et al. (60): the chemistry of the dosimeter was evaluated against the influence of oxygen concentration, depletion of oxygen, C3CA concentration and other factors. Additionally, pulse radiolysis experiments have been performed in order to determine the rate constant for the initiating hydroxyl radical scavenging reaction by the C3CA anion [determined in (60) to be 6.8×10^9 M^{-1} s^{-1}]. In the experiments where oxygen was absent in the solutions, formation of the hydroxylated C3CA molecule proceeded by disproportionation only, since the peroxylation step was not possible, which was in agreement with an up to 50% drop of the fluorescence yield. The authors have analyzed their results using a numeric model where they assumed that in the absence of O_2 the reaction proceeded via the disproportionation reaction when two intermediate hydroxy-dienyl radicals meet and disproportionate to form one unhydroxylated and one hydroxylated C3CA molecule.

In their model, Yamashita et al. (60) assumed that both the peroxylation reaction of the hydroxy-dienyl radical with the oxygen molecule and the bimolecular disproportionation reaction have the same rate constant $k_{+O2} = k_{disp.} = 10^9$ M^{-1} s^{-1} and that the $HO_2^\bullet$ elimination reaction follows immediately after the peroxylation step so that the oxygenated pathway is essentially complete within 10^{-5} s, while in the absence of O_2 the disproportionation pathway would take up to $\sim 10^{-1}$ s (depending on the dose in the radiation pulse) (60). However, these assumptions do not mirror the experimental observations of the terephthalate system where the peroxylation (O_2 addition) rate constant value was measured as $k_{+O2,\ TER} = 1.6 \times 10^7$ M^{-1} s^{-1} (42). Consequently, the peroxylation step would apparently take much longer to complete [$\tau_{+O2\ ,\ TER} \approx k_{+O2,\ TER}^{-1} \bullet [O_2]^{-1} \approx 2 \times 10^{-4}$ s, assuming that $[O_2] \approx 3 \times 10^{-4}$ M (88)]. In addition, notably, the peroxylation step of the cyclohexadienyl radicals was observed to be highly reversible (92) and the reverse reaction (O_2 elimination) in the terephthalate system has been measured to be nearly tenfold faster than the $HO_2^\bullet$ elimination ($k_{-O2,\ TER} : k_{elim.,\ TER} = 8.7$) (42). Therefore, peroxylation does not go to completion, instead, a transient equilibrium is achieved where the concentrations of the reactants are governed by an apparent stability constant $K = k_{+O2}/k_{-O2} \approx [HO\text{-}RO_2^\bullet]/[HO\text{-}R^\bullet][O_2]$. For the aerated terephthalate system the value of the constant is $K_{TER} = 4.7 \times 10^3$ M^{-1} and the ratio $[HO\text{-}RO_2^\bullet]$:$[HO\text{-}R^\bullet]$ is equal to 1.4; this means that in the stationary state the populations of peroxylated and unperoxylated OH-adducts are nearly equal. The lifetime of the peroxyl radical under the monomolecular $HO_2^\bullet$ elimination reaction would be $\tau_{elim.,\ TER} \approx k_{elim.TER}^{-1} = 2.6 \times 10^{-3}$ s, approximately 10× longer than how long it approximately takes for the initial peroxylation to achieve completion.

In this model, the dosimeter yield is being governed by the competition between the rates of disproportionation and of $HO_2^\bullet$ elimination. The disproportionation reaction has the effect of reduction of the total yield of fluorescent products originating from the generated $OH^\bullet$. Since it is a bimolecular reaction, its rate is proportional to $[HO\text{-}R^\bullet]^2$. At low dose rates the $[HO\text{-}R^\bullet]^2$ would be very small and the elimination branch is much faster, for terephthalate this has been shown to be true for doses below approximately 1 Gy/pulse (42) and is in line with the results presented here. However, at high dose rates the initial bimolecular disproportionation rate will approach the monomolecular rate of elimination ($k_{disp.}[HO\text{-}R^\bullet]^2 \approx k_{elim.}[HO\text{-}RO_2^\bullet]$), resulting in significant reduction of the yield of the fluorescence dosimeter.

The reversible reaction kinetics of O_2 addition on cyclohexadienyl radicals produced by aromatic substitution has been studied in depth by Clemens von Sonntag and collaborators (92–94). The values of k_{+O2}, k_{-O2} and $k_{elim.}$ were found to vary significantly depending on the aromatic ring substituents, with electron-withdrawing substituents considerably slowing down both the rate of O_2 addition as well as the rate of elimination (92, 94). For instance, in the nitrobenzene system and benzonitrile systems the peroxylation rates were observed to be so low [values of k_{+O2} were 2×10^6 and 5×10^6 $M^{-1}s^{-1}$, respectively (92)] that they did not even permit to determine k_{-O2} and $k_{elim.}$ using pulse radiolysis methods, the half-life of the bimolecular disproportionation was several times shorter than the rate of O_2 addition in even the lowest pulsed doses utilized (92) (which also indicates

that the value of $k_{disp.}$ was likely higher than in the terephthalate system, above 10^9 M^{-1} s^{-1}). For the C3CA molecule only the rate constant for $OH^{\bullet}$ addition is known in the mechanism in Fig. 12, but the presence of the electron-withdrawing carbonyl and carboxyl groups on the pyranone ring of the C3CA molecule permits one to propose that both k_{+O2} and $k_{elim.}$ could be even lower than they are in the case of the terephthalate system, which would then render the yield of the system much more sensitive to the increase of the dose rate. Such shifts in the values of the relevant rate constants could result in the disproportionation pathway becoming dominant already at relatively low dose rates and, hence, explain the ~60% yield drops of the C3CA dosimeter that takes place over an increase of dose rate from 0.1 to 10 Gy/s measured by Kusumoto et al. (73) and a very similar yield reduction registered for the smallest doses used in this study. The reason why the reductions in the C3CA yield surpass 50% is probably caused by the fact that a minor proportion of the bimolecular radical combination/disproportionation reactions do not follow exactly the simplified scheme in Fig. 12, so on average less than one HO-C3CA molecule is produced per two HO-C3CA$^{\bullet}$ radicals consumed. To verify these hypotheses a more detailed pulse radiolysis study would need to be performed, likely supported by a study of the impact of dose rate on the chemical yields of other products of C3CA radiolysis and appropriate numerical modeling.

CONCLUSION

The ferrous sulfate (Fricke) dosimeter and three fluorescence liquid chemical dosimeters based on the solutions of terephthalic acid, trimesic acid and coumarin-3-carboxylic acid were utilized in order to investigate the effect of very high dose rates (10^{11}–10^{12} Gy/s) with low dose per pulse from picosecond pulses of low-LET radiation (4.5 MeV electrons) on their radiation chemical yield, compared to the yields characterized for low dose rates (10^{-3} Gy/s) by a 60 Co gamma-ray source. In earlier works on this topic investigating the Fricke dosimeter (18) and the coumarin dosimeters (57, 68) reductions in the yields were observed already at much smaller dose rates ($<10^6$ Gy/s). The results of the present work are that a significant and substantial 60% decrease of radiation-chemical yield was observed only for the fluorescence dosimeter based on solutions of coumarin-3-carboxylic acid. Meanwhile, changes in the yields for the Fricke, the terephthalate, and the trimesic acid dosimeters were not detected above the estimated (~10 %) overall measurement error of the experiments.

Due to the low-LET character of the radiation a hypothesis can be formulated that below a certain pulse length ($<10^{-6}$ s) the yield is not determined by the dose rate, but by the total dose delivered to the liquid system over the duration of the radiation pulse. A threshold dose, specific to each dosimetric system, may then exist, above which changes in the chemical yields would manifest, regardless of the pulse length. In particular, when the pulsed beam is used, the radical-radical reactions in homogenous step become important and the yield can be affected. In that case, the scavenging time is decisive. The hypothesis should be tested by follow-up experiments that would map more densely the range of dose at high dose rate and by studies of the topic based on kinetic modeling and simulations that would help to formulate the problem in a more quantitative manner.

SUPPLEMENTARY INFORMATION

This article is accompanied by a supplementary document that contains extended description of the spectrofluorimetric measurements.

ACKNOWLEDGMENTS

This research was supported by the project Advanced research using high intensity laser produced photons and particles (ADONIS) (CZ.02.1.01/0.0/0.0/16_019/0000789) from European Regional Development Fund and received funding from the European Union's Horizon 2020 research and innovation programme under grant agreement no. 871124 Laserlab-Europe. At the Czech local funding, a financial support was obtained from the Czech Science Foundation (grant nr. 19-03314S), while LV thanks the Czech Academy of Sciences for a financial support provided within the program PPLZ 2020.

Received: December 22, 2020; accepted: September 7, 2021; published online: October 6, 2021

REFERENCES

1. Ackermann W, Asova G, Ayvazyan V, Azima A, Baboi N, Bähr J, et al. Operation of a free-electron laser from the extreme ultraviolet to the water window. Nat Photonics. 2007 Jun 1; 1(6):336–42.
2. Emma P, Akre R, Arthur J, Bionta R, Bostedt C, Bozek J, et al. First lasing and operation of an ångstrom-wavelength free-electron laser. Nat Photonics. 2010; 4(9):641–7.
3. Murnane MM, Kapteyn HC, Gordon SP, Falcone RW. Ultrashort X-ray pulses. Appl Phys B. 1994; 58(3):261–6.
4. Malka V, Faure J, Glinec Y, Lifschitz A. Laser–plasma accelerator: status and perspectives. Philos Trans R Soc A Math Phys Eng Sci. 2006 Mar 15; 364(1840):601–10.
5. Borghesi M, Fuchs J, Bulanov S V., Mackinnon AJ, Patel PK, Roth M. Fast ion generation by high-intensity laser irradiation of solid targets and applications. Fusion Sci Technol. 2006; 49(3):412–39.
6. Belloni J, Crowell RA, Katsumura Y, Lin M, Marignier J-L, Mostafavi M, et al. Ultrafast pulse radiolysis methods. In: Wishart JF, Rao BSM, editors. Recent Trends in Radiation Chemistry. Singapore: World Scientific Publishing Co. Pte. Ltd. 2010. p. 121–60.
7. Papadogiannis NA, Witzel B, Kalpouzos C, Charalambidis D. Observation of attosecond light localization in higher order harmonic generation. Phys Rev Lett. 1999 Nov 22; 83(21):4289–92.
8. Huang S, Ding Y, Feng Y, Hemsing E, Huang Z, Krzywinski J, et al. Generating single-spike hard X-ray pulses with nonlinear bunch compression in free-electron lasers. Phys Rev Lett. 2017; 119(15):1–6.
9. Karsch L, Beyreuther E, Enghardt W, Gotz M, Masood U, Schramm U, et al. Towards ion beam therapy based on laser plasma accelerators. Acta Oncol (Madr). 2017; 56(11):1359–66.
10. Kokurewicz K, Brunetti E, Welsh GH, Wiggins SM, Boyd M,

Sorensen A, et al. Focused very high-energy electron beams as a novel radiotherapy modality for producing high-dose volumetric elements. Sci Rep. 2019; 9(1):1–10.

11. Allen AO. Variations of the molecular and radical yields with type of radiation with solute concentration. In: The Radiation Chemistry of Water and Aqueous Solutions. Princeton, N.J.: Van Nostrand; 1961.

12. Mozumder A. Ionization and excitation phenomena. In: Fundamentals of Radiation Chemistry. Academic Press, Inc. 1999. p. 71–120.

13. Schuler RH, Allen AO. Yield of the ferrous sulfate radiation dosimeter: an improved cathode-ray determination. J Chem Phys. 1956 Jan; 24(1):56–9.

14. Keene JP. The oxidation of ferrous ammonium sulfate solutions by electron irradiation at high dose rates. Radiat Res. 1957 Apr; 6(4):424.

15. Rotblat J, Sutton HC. The effects of high dose rates of ionizing radiations on solutions of iron and cerium salts. Proc R Soc London Ser A Math Phys Sci. 1960 May 10; 255(1283):490–508.

16. Glazunov PY, Pikaev AK. An investigation of the radiolytic oxidation of divalent iron with irradiation doses of high power. Dokl Akad Nauk SSSR. 1960; 130(5):1051–4.

17. Anderson AR. A calorimetric determination of the oxidation yield of the fricke dosimeter at high dose rates of electrons. J Phys Chem. 1962 Jan; 66(1):180–2.

18. Thomas JK, Hart EJ. The radiolysis of aqueous solutions at high intensities. Radiat Res. 1962 Sep; 17(3):408.

19. Al-Rawi AM, Aleh MM, Al-Meshadani NAF, Al-Fakhri KAK. Pulsed electrons of ultrahigh dose-rate effect in decrasing ferric ions of a Fricke dosimeter. Radiat Phys Chem. 1983 Jan; 22(3–5):295–304.

20. O'Leary M, Boscolo D, Breslin N, Brown JMC, Dolbnya IP, Emerson C, et al. Observation of dose-rate dependence in a Fricke dosimeter irradiated at low dose rates with monoenergetic X-rays. Sci Rep. 2018; 8(1).

21. Vyšín L, Wachulak P, Toufarová M, Medvedev N, Voronkov RA, Bartnik A, et al. Chemical dosimetry in the ''water window'': ferric ions and hydroxyl radicals produced by intense soft X rays. Radiat Res. 2020 Feb 25; 193(4):372.

22. ASTM. Standard practice for using the Fricke reference standard dosimetry system. West Conshohocken, PA; 1995.

23. Feng PY, Brynjolfsson A, Halliday JW, Jarrett RD. High-intensity radiolysis of aqueous ferrous sulfate-cupric sulfate-sulfuric acid solutions. J Phys Chem. 1970 Mar; 74(6):1221–7.

24. Khusnulina A. Researching the possibility to use Fricke dosimeter for measurement of absorbed dose generated by pulse electron beam. IOP Conf Ser Mater Sci Eng. 2014 Oct 7; 66:012032.

25. Gupta BL, Bhat RM, Gomathy KR, Susheela B. Radiation chemistry of the ferrous sulfate-benzoic acid-xylenol orange system. Radiat Res. 1978 Aug; 75(2):269.

26. Matthews RW. Aqueous chemical dosimetry. Int J Appl Radiat Isot. 1982; 33(11):1159–70.

27. Gupta BL, Kini UR, Bhat RM, Madhvanath U. Use of the FBX dosemeter for the calibration of cobalt-60 and high-energy teletherapy machines. Phys Med Biol. 1982; 27(2):235–45.

28. Moussous O, Medjadj T, Khoudri S. Dosimetric proprieties of FBX dosimeter for high energy photon and electron beams. Polish J Med Phys Eng. 2017; 23(3):55–9.

29. Gupta BL, Madhvanath U. G(Fe3+) values in the FBX dosimeter at low dose-rates. Int J Appl Radiat Isot. 1985 Dec; 36(12):985–7.

30. Nadrowitz R, Coray A, Boehringer T, Dunst J, Rades D. A liquid fluorescence dosimeter for proton dosimetry. Phys Med Biol. 2012; 57(5):1325–33.

31. Sicard-Roselli C, Brun E, Gilles M, Baldacchino G, Kelsey C, McQuaid H, et al. A new mechanism for hydroxyl radical production in irradiated nanoparticle solutions. Small. 2014; 10(16):3338–46.

32. Maeyama T, Hase S. Nanoclay gel-based radio-fluorogenic gel dosimeters using various fluorescence probes. Radiat Phys Chem. 2018; 151(May):42–6.

33. Náfrádi M, Farkas L, Alapi T, Hernádi K, Kovács K, Wojnárovits L, et al. Application of coumarin and coumarin-3-carboxylic acid for the determination of hydroxyl radicals during different advanced oxidation processes. Radiat Phys Chem. 2020; 170(November 2019):108610.

34. Itagaki H. Fluorescence spectroscopy. In: Experimental Methods in Polymer Science. Elsevier; 2000. p. 155–260.

35. Ingle JD, Crouch SR. Spectrochemical analysis. Englewood Cliffs, New Jersey: Prentice-Hall, Inc. 1988.

36. Shanker N, Bane SL. Basic aspects of absorption and fluorescence spectroscopy and resonance energy transfer methods. Methods Cell Biol. 2008; 84(07):213–42.

37. Barr NF, Stark MB. The destruction of the fluorescence of quinine in acid solution by 250 kvp X-rays. Radiat Res. 1958; 9(1):89–90.

38. Armstrong WA, Grant DW. A highly sensitive chemical dosimeter for ionizing radiation. Nature. 1958; 182(4637):747–747.

39. Armstrong WA, Grant DW. The aqueous benzoate system as a sensitive dosimeter for ionizing radiations. Can J Chem. 1960; 38(6):845–50.

40. Gomes A, Fernandes E, Lima JLFC. Fluorescence probes used for detection of reactive oxygen species. J Biochem Biophys Methods. 2005 Dec; 65(2–3):45–80.

41. Mason TJ, Lorimer JP, Bates DM, Zhao Y. Dosimetry in sonochemistry: the use of aqueous terephthalate ion as a fluorescence monitor. Ultrason - Sonochemistry. 1994; 1(2):2–6.

42. Fang X, Mark G, von Sonntag C. OH radical formation by ultrasound in aqueous solutions Part I: the chemistry underlying the terephthalate dosimeter. Ultrason Sonochem. 1996 Feb; 3(1):57–63.

43. Mark G, Tauber A, Laupert R, Schuchmann H-P, Schulz D, Mues A, et al. OH-radical formation by ultrasound in aqueous solution – Part II: Terephthalate and Fricke dosimetry and the influence of various conditions on the sonolytic yield. Ultrason Sonochem. 1998 Jun; 5(2):41–52.

44. Barati AH, Mokhtari M, Mozdarani H, Bathaei SZ, Hassan ZM. Free hydroxyl radical dosimetry by using 1 MHz low level ultrasound waves. Iran J Radiat Res. 2006; 3(4):163–9.

45. Kim MJ, Pal S, Tak YK, Lee KH, Yang TK, Lee SJ, et al. Determination of the dose-depth distribution of proton beam using resazurin assay in vitro and diode laser-induced fluorescence detection. Anal Chim Acta. 2007; 593(2):214–23.

46. Balcerzyk A, Baldacchino G. Implementation of laser induced fluorescence in a pulse radiolysis experiment - A new way to analyze resazurin-like reduction mechanisms. Analyst. 2014; 139(7):1707–12.

47. Armstrong WA, Facey RA, Grant DW, Humphreys WG. A tissue-equivalent chemical dosimeter sensitive to 1 rad. Can J Chem. 1963 Jun; 41(6):1575–7.

48. Matthews RW, Barker NT, Sangster DF. A comparison of some aqueous chemical dosimeters for absorbed doses of less than 1000 rads. Int J Appl Radiat Isot. 1978 Jan; 29(1):1–8.

49. Matthews RW. The radiation chemistry of the terephthalate dosimeter. Radiat Res. 1980; 83(1):27.

50. Saran M, Summer KH. Assaying for hydroxyl radicals: Hydroxylated terephthalate is a superior fluorescence marker than hydroxylated benzoate. Free Radic Res. 1999 Jan 7; 31(5):429–36.

51. Lide DR, editor. Dissociation constants of organic acids and bases. In: CRC Handbook of Chemistry and Physics, 88th edition. 88th ed. Boca Raton, FL: CRC Press/Taylor and Francis; 2007. p. 8–47.

52. Sheehan RJ. Terephthalic acid, dimethyl terephthalate, and isophthalic acid. In: Ullmann's Encyclopedia of Industrial

Chemistry. Weinheim, Germany: Wiley-VCH Verlag GmbH & Co. KGaA; 2011. p. 17–27.

53. Matthews RW. Trimesic acid—a fluorescence dosimeter for 1 to 1000 rad. Int J Appl Radiat Isot. 1980 Sep; 31(9):585–6.

54. Matthews RW, Wilson JG. Chemical dosimetry at less than 1000 rad: Aqueous trimesic acid solutions. Int J Appl Radiat Isot. 1981 May; 32(5):295–301.

55. Lakowicz JR. Principles of fluorescence spectroscopy. 3rd ed. Principles of Fluorescence Spectroscopy. Boston, MA: Springer US; 2006. 1–954 p.

56. Gopakumar K, Kini UR, Ashawa SC, Bhandari NS, Krishnan GU, Krishnan D. Gamma irradiation of coumarin in aqueous solution. Radiat Eff. 1977 Jan; 32(3–4):199–203.

57. Ashawa SC, Kini UR, Madhvanath U. The aqueous coumarin system as a low range chemical dosimeter. Int J Appl Radiat Isot. 1979; 30(1):7–10.

58. Manevich Y, Held KD, Biaglow JE. Coumarin-3-carboxylic acid as a detector for hydroxyl radicals generated chemically and by gamma radiation. Radiat Res. 1997 Dec; 148(6):580–91.

59. Makrigiorgos GM, Baranowska-Kortylewicz J, Bump E, Sahu SK, Berman RM, Kassis AI. A method for detection of hydroxyl radicals in the vicinity of biomolecules using radiation-induced fluorescence of coumarin. Int J Radiat Biol. 1993; 63(4):445–58.

60. Yamashita S, Baldacchino G, Maeyama T, Taguchi M, Muroya Y, Lin M, et al. Mechanism of radiation-induced reactions in aqueous solution of coumarin-3-carboxylic acid: Effects of concentration, gas and additive on fluorescent product yield. Free Radic Res. 2012 Jul 9; 46(7):861–71.

61. Boisde PM, Meuly WC, Staff U by. Coumarin. In: Kirk-Othmer Encyclopedia of Chemical Technology. Hoboken, NJ, USA: John Wiley & Sons, Inc.; 2014. p. 1–10.

62. Baldacchino G, Maeyama T, Yamashita S, Taguchi M, Kimura A, Katsumura Y, et al. Determination of the time-dependent OH-yield by using a fluorescent probe. Application to heavy ion irradiation. Chem Phys Lett. 2009; 468(4–6):275–9.

63. Sandwall PA. Spatial dosimetry with violet diode laser-induced fluorescence of water-equivalent radio-fluorogenic gels. University of Cincinnati; 2014.

64. Kimura A, Matsufuji N, Hiroki A, Seito H, Taguchi M. Development of high-sensitivity intra-corporeal catheter-type liquid dosimeter for radiotherapy. Biomed Phys Eng Express. 2018 Jul 26; 4(5):055005.

65. Tomanová K, Precek M, Múčka V, Vyšín L, Juha L, Čuba V. At the crossroad of photochemistry and radiation chemistry: formation of hydroxyl radicals in diluted aqueous solutions exposed to ultraviolet radiation. Phys Chem Chem Phys. 2017; 19(43):29402–8.

66. Newton GL, Milligan JR. Fluorescence detection of hydroxyl radicals. Radiat Phys Chem. 2006; 75(4):473–8.

67. Louit G, Foley S, Cabillic J, Coffigny H, Taran F, Valleix A, et al. The reaction of coumarin with the OH radical revisited: Hydroxylation product analysis determined by fluorescence and chromatography. Radiat Phys Chem. 2005; 72(2–3):119–24.

68. Collins AK, Makrigiorgos GM, Svensson GK. Coumarin chemical dosimeter for radiation therapy. Med Phys. 1994 Nov; 21(11):1741–7.

69. Louit G. New fluorescent probes of the hydroxyl radical: characterisation and modelization of the reactivity of coumarin derivatives with HO; Developpement de sondes fluorescentes du radical hydroxyle: caracterisation et modelisation de la reactivite de molecules. Universite Paris XI, Orsay, France; 2005.

70. Maeyama T, Yamashita S, Taguchi M, Baldacchino G, Sihver L, Murakami T, et al. Production of a fluorescence probe in ion-beam radiolysis of aqueous coumarin-3-carboxylic acid solution—2: Effects of nuclear fragmentation and its simulation with PHITS. Radiat Phys Chem. 2011 Dec; 80(12):1352–7.

71. Maeyama T, Yamashita S, Baldacchino G, Taguchi M, Kimura A, Murakami T, et al. Production of a fluorescence probe in ion-beam radiolysis of aqueous coumarin-3-carboxylic acid solution—1: Beam quality and concentration dependences. Radiat Phys Chem. 2011 Apr; 80(4):535–9.

72. Larochelle EPM, Shell JR, Gunn JR, Davis SC, Pogue BW. Signal intensity analysis and optimization for in vivo imaging of Cherenkov and excited luminescence. Phys Med Biol. 2018; 63(8).

73. Kusumoto T, Kitamura H, Hojo S, Konishi T, Kodaira S. Significant changes in yields of 7-hydroxy-coumarin-3-carboxylic acid produced under FLASH radiotherapy conditions. RSC Adv. 2020; 10(63):38709–14.

74. Belloni J, Monard H, Gobert F, Larbre J-P, Demarque a., De Waele V, et al. ELYSE—A picosecond electron accelerator for pulse radiolysis research. Nucl Instruments Methods Phys Res Sect A Accel Spectrometers, Detect Assoc Equip. 2005 Mar; 539(3):527–39.

75. Marignier J-L, de Waele V, Monard H, Gobert F, Larbre J-P, Demarque a., et al. Time-resolved spectroscopy at the picosecond laser-triggered electron accelerator ELYSE. Radiat Phys Chem. 2006 Sep; 75(9):1024–33.

76. Muroya Y, Lin M, Han Z, Kumagai Y, Sakumi A, Ueda T, et al. Ultra-fast pulse radiolysis: A review of the recent system progress and its application to study on initial yields and solvation processes of solvated electrons in various kinds of alcohols. Radiat Phys Chem. 2008; 77(10–12):1176–82.

77. Allison J, Amako K, Apostolakis J, Arce P, Asai M, Aso T, et al. Recent developments in Geant4. Nucl Instruments Methods Phys Res Sect A Accel Spectrometers, Detect Assoc Equip. 2016 Nov; 835:186–225.

78. Schneider CA, Rasband WS, Eliceiri KW. NIH Image to ImageJ: 25 years of image analysis. Nat Methods. 2012 Jul 28; 9(7):671–5.

79. Berger MJ, Coursey JS, Zucker MA, Chang J, Berger MJ, Coursey JS, Zucker MA, Chang J. ESTAR, PSTAR, and ASTAR: Computer programs for calculating stopping-power and range tables for electrons, protons, and helium ions (version 2.0.1) [Internet]. NIST Standard Reference Database 124. 2020 [cited 2020 May 1]. Available from: http://www.nist.gov/pml/data/star/index.cfm

80. Lumpkin AH, Yang BX, Berg WJ, White M, Lewellen JW, Milton SV. Optical techniques for electron-beam characterizations on the APS SASE FEL project. Nucl Instruments Methods Phys Res Sect A Accel Spectrometers, Detect Assoc Equip. 1999 Jun; 429(1–3):336–40.

81. Krzywinski J, Andrejczuk A, Bionta RM, Burian T, Chalupský J, Jurek M, et al. Saturation of a Ce:Y_3Al_5O_12 scintillator response to ultra-short pulses of extreme ultraviolet soft X-ray and X-ray laser radiation. Opt Mater Express. 2017 Mar 1; 7(3):665.

82. Trumbore CN, Youngblade W, Short DR. Computer modeling of data from pulse radiolysis studies of aqueous solutions containing scavengers of spur intermediates. J Phys Chem. 1984; 88(21):5057–61.

83. Trumbore CN, Youngblade W, Short DR. Computer modeling studies of the molecular product and ferric ion yields in the radiolysis of water and aqueous solutions with high energy electrons. Int J Radiat Appl Instrumentation Part. 1986; 28(4):349–54.

84. Pimblott SM, LaVerne JA, Mozumder A. Monte Carlo simulation of range and energy deposition by electrons in gaseous and liquid water. J Phys Chem. 1996; 100(20):8595–606.

85. Burns WG, Sims HE, Goodall JAB. Radiation chemical diffusion kinetic calculations with prescribed and non-prescribed diffusion-I. Spherical and cylindrical cases. Radiat Phys Chem. 1984; 23(1–2):143–80.

86. Bielski BHJ, Willson RL. Fast Kinetic Studies of Dioxygen-Derived Species and Their Metal Complexes. Philos Trans R Soc Lond B Biol Sci. 1985; 311(1152):473–82.

87. Ershov BG, Gordeev A V. A model for radiolysis of water and

aqueous solutions of H2, H2O2 and O2. Radiat Phys Chem. 2008; 77(8):928–35.

88. Weiss RF. The solubility of nitrogen, oxygen and argon in water and seawater. Deep Sea Res Oceanogr Abstr. 1970 Aug; 17(4):721–35.

89. Weiss H, Epp ER, Heslin JM, Ling CC, Santomasso A. Oxygen depletion in cells irradiated at ultra-high dose-rates and at conventional dose-rates. Int J Radiat Biol. 1974; 26(1):17–29.

90. Dorfman LM, Taub IA, Bühler RE. Pulse radiolysis studies. I. Transient spectra and reaction-rate constants in irradiated aqueous solutions of benzene. J Chem Phys. 1962 Jun; 36(11):3051–61.

91. Anbar M, Meyerstein D, Neta P. The reactivity of aromatic compounds toward hydroxyl radicals. J Phys Chem. 1966 Aug 1; 70(8):2660–2.

92. Fang X, Pan X, Rahmann A, Schuchmann H, von Sonntag C. Reversibility in the Reaction of Cyclohexadienyl Radicals with Oxygen in Aqueous Solution. Chem - A Eur J. 1995 Oct; 1(7):423–9.

93. Pan XM, Schuchmann MN, Von Sonntag C. Oxidation of benzene by the OH radical. A product and pulse radiolysis study in oxygenated aqueous solution. J Chem Soc Perkin Trans 2. 1993; (3):289–97.

94. Naumov S, von Sonntag C. UV-visible absorption spectra of alkyl-, vinyl-, aryl- and thiylperoxyl radicals and some related radicals in aqueous solution: a quantum-chemical study. J Phys Org Chem. 2005 Jul; 18(7):586–94.